Mutations in *CDC45*, Encoding an Essential Component of the Pre-initiation Complex, Cause Meier-Gorlin Syndrome and Craniosynostosis

Aimee L. Fenwick,[1,18] Maciej Kliszczak,[1,2,18] Fay Cooper,[3,18] Jennie Murray,[3] Luis Sanchez-Pulido,[3] Stephen R.F. Twigg,[1] Anne Goriely,[1] Simon J. McGowan,[4] Kerry A. Miller,[1] Indira B. Taylor,[1] Clare Logan,[3] WGS500 Consortium, Sevcan Bozdogan,[5] Sumita Danda,[6] Joanne Dixon,[7] Solaf M. Elsayed,[8] Ezzat Elsobky,[8] Alice Gardham,[9] Mariette J.V. Hoffer,[10] Marije Koopmans,[10] Donna M. McDonald-McGinn,[11] Gijs W.E. Santen,[10] Ravi Savarirayan,[12] Deepthi de Silva,[13] Olivier Vanakker,[14] Steven A. Wall,[15] Louise C. Wilson,[9] Ozge Ozalp Yuregir,[16] Elaine H. Zackai,[11] Chris P. Ponting,[3] Andrew P. Jackson,[3,19] Andrew O.M. Wilkie,[1,15,19] Wojciech Niedzwiedz,[2,*] and Louise S. Bicknell[3,17,*]

DNA replication precisely duplicates the genome to ensure stable inheritance of genetic information. Impaired licensing of origins of replication during the G_1 phase of the cell cycle has been implicated in Meier-Gorlin syndrome (MGS), a disorder defined by the triad of short stature, microtia, and a/hypoplastic patellae. Biallelic partial loss-of-function mutations in multiple components of the pre-replication complex (preRC; *ORC1*, *ORC4*, *ORC6*, *CDT1*, or *CDC6*) as well as de novo stabilizing mutations in the licensing inhibitor, *GMNN*, cause MGS. Here we report the identification of mutations in *CDC45* in 15 affected individuals from 12 families with MGS and/or craniosynostosis. *CDC45* encodes a component of both the pre-initiation (preIC) and CMG helicase complexes, required for initiation of DNA replication origin firing and ongoing DNA synthesis during S-phase itself, respectively, and hence is functionally distinct from previously identified MGS-associated genes. The phenotypes of affected individuals range from syndromic coronal craniosynostosis to severe growth restriction, fulfilling diagnostic criteria for Meier-Gorlin syndrome. All mutations identified were biallelic and included synonymous mutations altering splicing of physiological *CDC45* transcripts, as well as amino acid substitutions expected to result in partial loss of function. Functionally, mutations reduce levels of full-length transcripts and protein in subject cells, consistent with partial loss of CDC45 function and a predicted limited rate of DNA replication and cell proliferation. Our findings therefore implicate the preIC as an additional protein complex involved in the etiology of MGS and connect the core cellular machinery of genome replication with growth, chondrogenesis, and cranial suture homeostasis.

Introduction

Replication of DNA during eukaryotic cell division is an essential process, which requires a complex apparatus of conserved proteins operating under tight temporal and regulatory control. Although the duplication process itself occurs during the S (synthesis) phase of the cell cycle, the initial components assemble on DNA much earlier, during the late mitotic stages and in G_1 phase.

In the first stage, the pre-replication complex (preRC) is formed by the 6-subunit origin recognition complex (ORC) binding to replication origins distributed throughout the genome (Figure 1).[1] ORC recruits CDT1 and CDC6, which leads to the binding of the inactive MCM2-7 helicase as a double hexamer at replication origins.[2] At the G_1/S transition, the pre-initiation complex (preIC) proteins assemble in a two-step DDK- and CDK-dependent manner[3] and through interaction with the MCM helicase enable binding by the CDC45 and GINS1-4 proteins. This creates the activated CMG helicase, an 11-subunit complex that possesses essential DNA unwinding activity, allowing polymerases access to DNA and enabling replication to commence.[4–8] CDC45 has single-stranded DNA binding activity, facilitating DNA strand displacement at the replication fork.[9]

[1]Clinical Genetics Group, MRC Weatherall Institute of Molecular Medicine, University of Oxford, John Radcliffe Hospital, Oxford OX3 9DS, UK; [2]Department of Oncology, MRC Weatherall Institute of Molecular Medicine, University of Oxford, Oxford OX3 9DS, UK; [3]MRC Human Genetics Unit, IGMM, University of Edinburgh, Edinburgh EH4 2XU, UK; [4]Computational Biology Research Group, MRC Weatherall Institute of Molecular Medicine, University of Oxford, John Radcliffe Hospital, Oxford OX3 9DS, UK; [5]Department of Medical Genetics, Mersin University, Mersin, 33343 Cukurova, Turkey; [6]Department of Clinical Genetics, Christian Medical College and Hospital, Vellore, Tamil Nadu 632004, India; [7]Genetic Health Service NZ-South Island Hub, Christchurch Hospital, Christchurch, Canterbury 8140, New Zealand; [8]Children's Hospital, Ain Shams University, Cairo 11566, Egypt; [9]North East Thames Regional Genetics Service, Great Ormond Street Hospital for Children NHS Foundation Trust, Great Ormond Street Hospital, London WC1N 3JH, UK; [10]Department of Clinical Genetics, Leiden University Medical Center, 2300 RC Leiden, the Netherlands; [11]Clinical Genetics, The Children's Hospital of Philadelphia, 34th & Civic Center Boulevard, Philadelphia, PA 19104, USA; [12]Victorian Clinical Genetics Services, Murdoch Children's Research Institute, University of Melbourne, Melbourne, VIC 3052, Australia; [13]Department of Physiology, Faculty of Medicine, University of Kelaniya, Ragama, Gampaha GQ 11010, Sri Lanka; [14]Center for Medical Genetics, Ghent University Hospital, 9000 Ghent, Belgium; [15]Craniofacial Unit, Department of Plastic and Reconstructive Surgery, Oxford University Hospitals NHS Foundation Trust, John Radcliffe Hospital, Oxford OX3 9DU, UK; [16]Genetic Diagnosis Center, Adana Numune Training and Research Hospital, Cukurova, Adana, 01170, Turkey; [17]Department of Pathology, Dunedin School of Medicine, University of Otago, Dunedin, Otago 9016, New Zealand
[18]These authors contributed equally to this work
[19]These authors contributed equally to this work and are co-senior authors
*Correspondence: wojciech.niedzwiedz@imm.ox.ac.uk (W.N.), louise.bicknell@otago.ac.nz (L.S.B.)
http://dx.doi.org/10.1016/j.ajhg.2016.05.019.

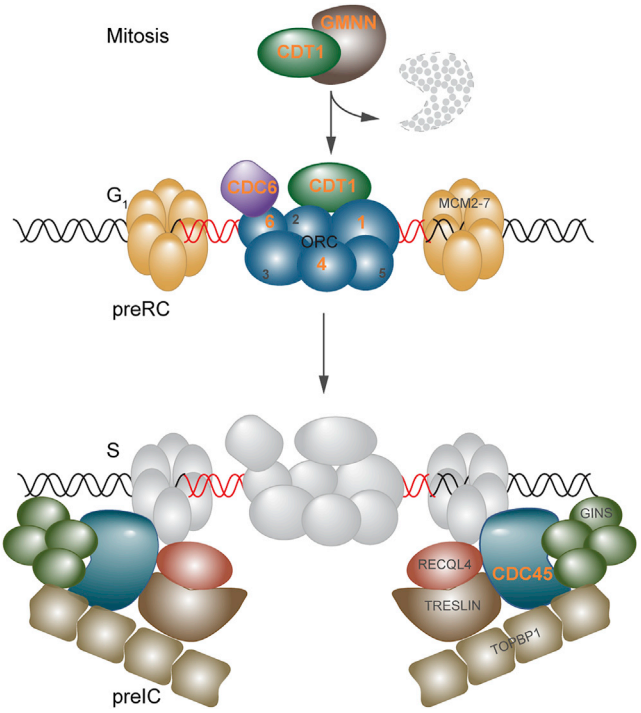

Figure 1. Pre-replication and Pre-initiation Complexes in DNA Replication, Showing Components Mutant in MGS
Previously identified MGS-associated genes (labeled with orange lettering) encode members of the pre-replication complex (preRC, upper cartoon); these components are involved in the licensing of replication origins during the G_1 phase of the cell cycle. GMNN acts during other cell cycle phases to inhibit CDT1 but is degraded in late M (mitosis) phase (indicated by GMNN with dashed outline), permitting free CDT1 to participate in origin licensing in G_1. In contrast, CDC45 contributes at the next major step in DNA replication, in which the coordinated action of many replication initiation factors including RECQL4 forms the pre-initiation complex (preIC, lower cartoon) to support the interaction of CDC45 and GINS1-4 with the MCM helicase, converting the latent form to an active helicase and initiating the unwinding of DNA.

Hence CDC45 plays a central role in both initiation of DNA replication origin firing (preIC) and ongoing DNA synthesis (CMG helicase), and genetic studies demonstrate that it is essential in both yeast and mice.[10–14] Both in vitro and in vivo data indicate that CDC45 is loaded onto chromatin specifically in the S phase of the cell cycle, after the assembly of the preRC complexes.[11,14–17]

Several Mendelian syndromes have been associated with mutations in components of the DNA replication machinery. Meier-Gorlin syndrome (MGS [MIM: 224690]) is characterized by short stature, microtia (small ears), and aplasia or hypoplasia of the patellae.[18] Biallelic mutations in multiple components of the preRC (*ORC1* [MIM: 601902], *ORC4* [MIM: 603056], *ORC6* [MIM: 607213], *CDT1* [MIM: 605525], and *CDC6* [MIM: 602627]) were identified in individuals with MGS,[19–21] and among them, mutations in these genes account for approximately 70% of cases.[22] Recently, de novo mutations in three individuals were reported in the CDT1 inhibitor, *GMNN* (MIM: 602842), resulting in the omission of a degron domain that stabilizes GMNN levels and is consequently predicted to impair licensing in subject cells.[23,24]

Here, we provide genetic and functional evidence that mutations in *CDC45* (MIM: 603465) cause human disease. We describe 15 individuals with biallelic partial loss-of-function mutations in *CDC45* and demonstrate a phenotype that extends from syndromic craniosynostosis to classical MGS.

Subjects and Methods

Clinical Studies

The clinical studies were approved by Oxfordshire Research Ethics Committee B (reference C02.143), London Riverside Research Ethics Committee (reference 09/H0706/20), Scottish Multicenter Research Ethics Committee (04:MRE00/19), and the Medisch Ethische Toetsingscommissie of the Leiden University Medical Center (LUMC) (P14-029). Subjects were enrolled into the craniosynostosis cohort based on referral from a craniofacial unit or clinical genetics department, with craniosynostosis proven on either plain radiographs or computed tomography (CT) of the skull. Individuals in the MGS cohort were clinically diagnosed by the referring clinician; in those from whom clinical data were available, all demonstrated hypoplastic or absent kneecaps, small or simple ears, and facies typical of MGS (small mouth and full lips). All participants gave informed consent, and separate permission was obtained for publication of clinical photographs.

Whole-Genome and Exome Sequencing

Subjects P1 (family 1, II-3 in Figure 2A) and P2 (family 2, II-1 in Figure 2A), from a craniosynostosis cohort, were subjected to whole-genome sequencing and exome sequencing, respectively. Exome sequencing of subject P4 (family 4, II-1 in Figure 2A) was undertaken by Oxford Gene Technology, as part of a study of subjects with primordial dwarfism (characterized by in utero growth retardation and postnatal head circumference and height more than 4 SDs below the age- and gender-matched population mean). Exome sequencing of family 12 was undertaken as part of a diagnostic approach to mutation identification. All details of sequencing library preparations and platforms, as well as software tools for mapping, alignment, and variant calling and prioritization, are presented in Table S1.

Genomic Analysis of *CDC45*

To investigate further the significance of the *CDC45* variants, primers were designed for amplification of genomic DNA (GenBank: NT_011520.13) and cDNA (GenBank: NM_003504.4; see Supplemental Data, Note on accession numbers for *CDC45*). We used dideoxy sequencing to confirm the identity of *CDC45* variants identified during whole-genome and exome sequencing and analyzed their segregation in parents and unaffected siblings. Primer sequences and experimental conditions used for PCR amplification and sequencing are provided in Table S2. To analyze a larger number of individuals for *CDC45* mutations, we used Fluidigm/Ion Torrent resequencing or dideoxy sequencing, respectively, to screen *CDC45* in DNA panels from subjects with craniosynostosis (467 samples) or MGS (34 samples), in whom mutations

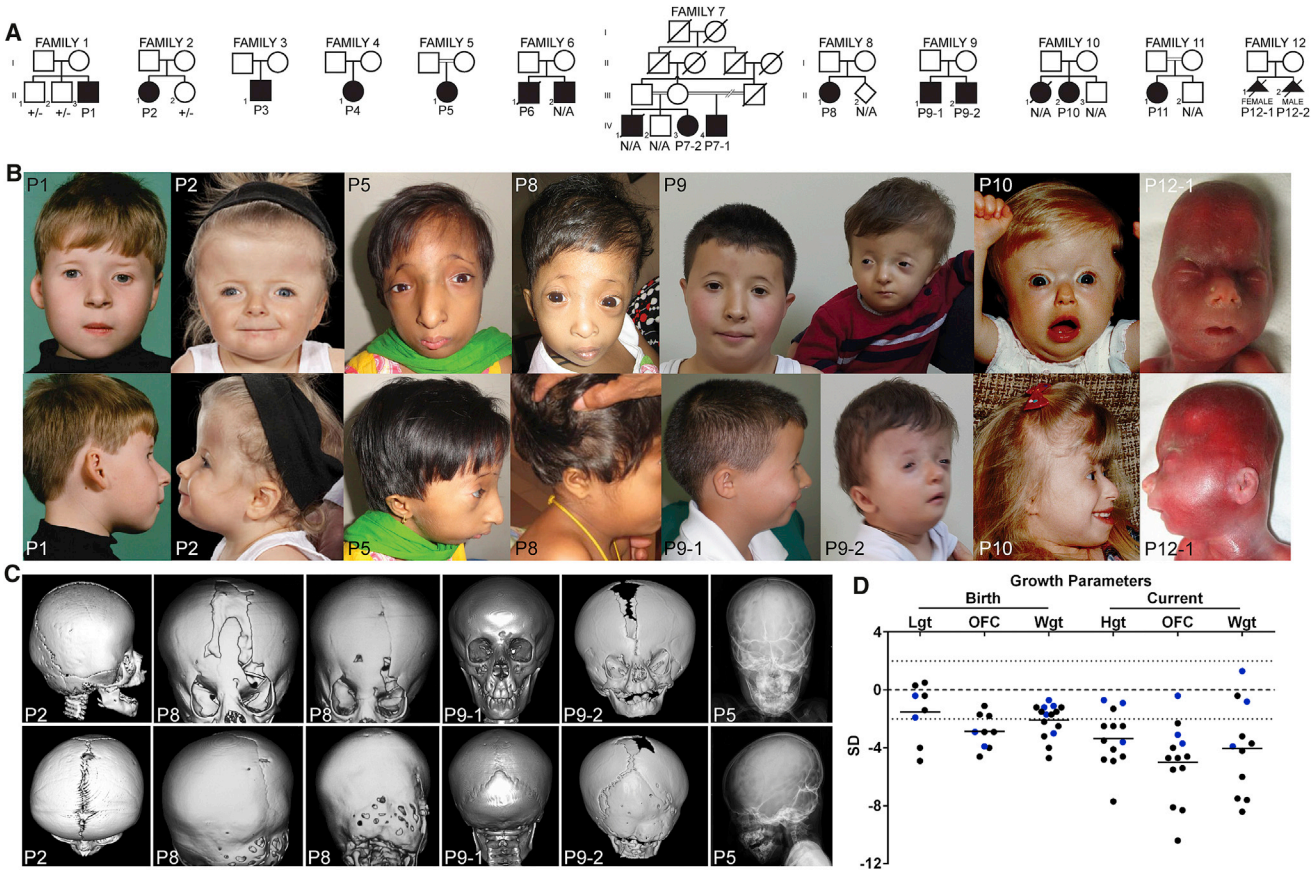

Figure 2. Clinical Features of Individuals with Mutations in *CDC45*

(A) Pedigrees of families segregating mutations in *CDC45*. Note consanguinity in families 5, 7, and 11 and that all parents and unaffected siblings available for testing were heterozygous for only one variant, consistent with autosomal-recessive inheritance.

(B) Facial appearance of individuals with *CDC45* mutations. Many individuals demonstrate the facial characteristics of MGS including microtia, small mouth, full lips, and micrognathia, but there is a marked spectrum of severity across the cohort. Note the consistent appearance of thin eyebrows.

(C) CT head scans and plain skull radiographs of individuals with *CDC45* mutations demonstrating premature fusion of cranial sutures. Note the discordance in suture fusion between sibs P9-1 and P9-2. Imaging of P8 indicates progressive suture closure (P8 left panel, age 2 years 4 months; P8 right panel, age 3 years 8 months). Skull radiography of P5 demonstrates a beaten-copper appearance of the skull.

(D) Individuals with *CDC45* mutations have below-average stature and many exhibited intrauterine growth retardation and microcephaly (both in utero and postnatally). Abbreviations are as follows: Lgt, length; OFC, occipitofrontal circumference; Wgt, weight; Hgt, height. Blue indicates individuals derived from craniosynostosis cohort; black indicates individuals derived from MGS cohort.

in known causative genes had not previously been identified (Table S2). Multiplex ligation-dependent probe amplification (MLPA) was used to confirm the intragenic deletion in family 12 (Table S2).

Analysis of *CDC45* Splicing

Total RNA was extracted from lymphoblastoid cell lines using Trizol reagent (Invitrogen) and the RNeasy kit (QIAGEN) according to the manufacturer's instructions. DNA was removed by treatment with DNase I (QIAGEN). cDNA was generated using random oligomer primers and superscript II (Thermo Fisher) or the RevertAid First Strand Synthesis kit (Fermentas). Primers used for RT-PCR and qRT-PCR are listed in Table S3. cDNA levels were quantified by qRT-PCR using Brilliant II SYBR green qPCR master mix with passive ROX reference dye (Agilent Technologies) on the ABI Prism HT7900 Sequence Detection System. The relative expression of target genes to a control was calculated using the comparative CT method ($2^{-\Delta\Delta CT}$).

Cell Lines, Chemicals, Plasmids, and Transfections

Lymphoblastoid cell lines were cultured in RPMI-1640 supplemented with 15% fetal bovine serum (FBS) and 1% penicillin and streptomycin. Amniocytes were cultured in Amnio-MAX C-100 Complete Medium (GIBCO). All reagents were purchased from Life Technologies unless otherwise stated.

Antibodies and Western Blotting

Whole-cell lysate was prepared using urea buffer (9 M urea, 50 mM Tris HCl [pH 7.3], 150 mM β-mercaptoethanol). Primary antibodies used were mouse anti-human CDC45 (sc55569, Santa Cruz Biotech) at 1:1,000 and mouse anti-human TUBULIN (B512, Sigma) at 1:10,000.

Protein Alignments and Structure Prediction

Clustal Omega[25] was used to generate multi-sequence alignments of orthologous CDC45 proteins. GenBank accession numbers

Table 1. Mutations Identified in *CDC45*

Subject	Country of Origin	Allele 1	Allele 2	Segregation
P1[a]	UK	c.318C>T, p.Val106= (SE)	c.677A>G, p.Asp226Gly	Het, M, P, (2)[b]
P2	UK	c.226A>C, p.Asn76His	c.469C>T, p.Arg157Cys	Het, M, P, (1)
P3	USA	c.653+5G>A (SE)	c.1487C>T, p.Pro496Leu	Het, M, P
P4	Bangladesh	c.1A>C, p.Met1?	c.1388C>T, p.Pro463Leu	nps
P5	Bangladesh	c.1270C>T, p.Arg424*	c.1388C>T, p.Pro463Leu	Het, M, P
P6	Belgium	c.791C>A, p.Ser264Tyr	c.791C>A, p.Ser264Tyr	Hom, M, P
P7-1	Egypt	c.1660C>T, p.Arg554Trp	c.1660C>T, p.Arg554Trp	Hom, M (P deceased)
P7-2	Egypt	c.1660C>T, p.Arg554Trp	c.1660C>T, p.Arg554Trp	Hom, M, P
P8	Sri Lanka	c.1388C>T, p.Pro463Leu	c.1532delC, p.Pro511Glnfs*36	Het, M, P
P9-1	Turkey	c.203A>G, p.Gln68Arg (SE)	c.333C>T, p.Asn111= (SE)	Het, M, P
P9-2	Turkey	c.203A>G, p.Gln68Arg (SE)	c.333C>T, p.Asn111= (SE)	Het, M, P
P10[c]	New Zealand	c.[464A>G; 961C>A], p.[Glu155Gly; Pro321Thr]	c.1440+14C>T (SE)	Het, M, P
P11	Egypt	c.1660C>T, p.Arg554Trp	c.1660C>T, p.Arg554Trp	Hom, M, P
P12-1	the Netherlands	c.(485+1_486−1)_(630+1_631−1) del, p.Ile115_Glu162del	c.893C>T, p.Ala298Val	Het, M, P
P12-2	the Netherlands	c.(485+1_486−1)_(630+1_631−1) del, p.Ile115_Glu162del	c.893C>T, p.Ala298Val	Het, M, P

Refseq accession: NM_003504.4. Abbreviations are as follows: SE, splicing effect; Het, compound heterozygous in affected individual; nps, no parental samples available; M, mutation identified in mother; P, mutation identified in father; Hom, homozygous in affected individual.
[a]Mutation previously reported[28] (note mutation numbering differs in previous publication due to different reference transcript).
[b]Numbers in parentheses indicate number of clinically unaffected siblings shown not to have inherited the compound heterozygous genotype.
[c]Subject P10 segregates two rare missense variants on one allele, in combination with a splice region mutation on the second allele. Based on conservation of CDC45 residues across different species, the p.Pro321Thr variant is more likely to be deleterious as this residue is conserved through to *S. cerevisiae* (Figure 3).

are as follows: *Homo sapiens*, NP_003495.1; *Pan troglodytes*, XP_009436063.1; *Canis lupus*, XP_543547.3; *Mus musculus*, NP_033992.2; *Gallus gallus*, XP_415070.2; *Danio rerio*, NP_998551.1; *Drosophila melanogaster*, NP_569880.1; *Anopheles gambiae*, XP_320573.1; *Caenorhabditis elegans*, NP_497756.2; *Saccharomyces cerevisiae*, NP_013204.1; and *Schizosaccharomyces pombe*, NP_594693.1. The structural model of human CDC45 was modeled on the 3.7 Å cryo-electron microscopy structure of *S. cerevisiae* Cdc45.[26] It was created using Modeler[27] and is presented using Pymol (Schrodinger).

Results

Exome and Genome Sequencing and Targeted Resequencing Identify Biallelic Variants in *CDC45*

As part of a large multi-disease study,[28] clinical whole-genome sequencing of a trio comprising a male individual (P1, family 1; II-3 in Figure 2A) with syndromic unilateral coronal craniosynostosis and his unaffected parents initially identified several candidate variants for further scrutiny. These were a single de novo missense mutation (*FLRT1* [MIM: 604806]; c.137C>T, p.Thr46Met [GenBank: NM_013280.4]), two very rare (absent in dbSNP135, ESP, or 1000 Genomes) hemizygous nonsynonymous variants (*OPHN1* [MIM: 300127]; c.1559C>T, p.Thr520Ile [GenBank: NM_002547.2]; and *GEMIN8* [MIM: 300962]; c.500G>A, p.Arg167His [GenBank: NM_017856.2]), and two very rare compound heterozygous genotypes: *CDC45* c.[318C>T; 677A>G], p.[Val106= ; Asp226Gly] and *MYO10* (MIM: 601481) c.[1491G>A; 5459A>C], p.[Glu497= ; His1820Pro] (GenBank: NM_012334.2). *FLRT1* was initially prioritized for further analysis, but resequencing this gene in a panel of 230 individuals with craniosynostosis revealed no further mutations. During concurrent exome sequencing of female subject P2 (family 2; II-1 in Figure 2A) with syndromic bilateral coronal craniosynostosis, variant analysis under a recessive model of inheritance also identified two very rare predicted missense changes in *CDC45* (c.226A>C [p.Asn76His] and c.469C>T [p.Arg157Cys]); dideoxy sequencing of parental samples showed that the *CDC45* variants were present in a compound heterozygous (biallelic) state. Given the identification of two individuals with unilateral or bilateral coronal or craniosynostosis, each of whom had two rare biallelic variants in *CDC45* (Table 1), resequencing of *CDC45* was undertaken in a further 467 subjects with craniosynostosis. This revealed one further individual (P3, family 3; II-1 in Figure 2A) with two rare *CDC45* variants (Table 1), which analysis of parental samples showed were also biallelic. Consistent with a causal role in the disease state, three unaffected siblings of P1 and P2 inherited different combinations of *CDC45* alleles (Figure 2A).

Table 2. Clinical Characteristics of Individuals with Mutations in *CDC45*

			Birth, SD				Current Exam, SD				MGS Features					
Subj.	Consan	Gender	Gest.	Lgt (cm)	OFC (cm)	Wgt (kg)	Age	Hgt (cm)	OFC (cm)	Wgt (kg)	Microtia	A/Hypoplastic Patella	Thin Eyebrows	Develop. Delay	Craniosynostosis	Other Clinical Features
P1	N	M	40	NA	NA	−0.7 (3.2)	28 years	−0.7 (173)	−0.4[a] (55.5)	+1.3 (85.7)	+	−	+	none	right unicoronal	urethral stricture, mild 2/3/4 syndactyly of hands
P2	N	F	38	NA	NA	−1.2 (2.5)	4 years 4 months	−0.9 (100)	−3.1 (47.6)	−0.8 (15.3)	−	−	+	none	bicoronal	anterior anus, bilateral strabismus
P3	N	M	38	NA	NA	−1.7 (2.4)	16 years 3 months	−3.6 (147)	−3.7 (50.5)	−3.9 (35.3)	+	−	+	mild	bicoronal	R choanal atresia, high palate, imperforate anus, vesicoureteral reflux, hypospadias, 2-3 syndactyly of toes, scoliosis, C1-C3 and C4-C7 fusion, bilateral radial head dislocation
P4	N	F	36	NA	−2.9 (28.5)	−3.2 (1.45)	5 years 5 months	−7.7[b] (48)	−8.3[b] (33)	−6.1 (9.9)	+	+	+	severe	large anterior fontanelle (X-ray)	cleft palate, exorbitism, bilateral radial head dislocation, thoracic vertebral segmentation defects, digital clubbing, pulmonary hypoplasia, anterior anus, cliteromegaly
P5	3rd	F	40	NA	NA	−4.7 (1.5)	6 years	−4.6 (93)	−8.1 (42.5)	−7.5 (9.2)	+	+	+	none	copper-beating on skull radiograph	cleft palate, bowed legs, anorectal malformation
P6	N	M	34	0.3 (46.5)	−1.1 (30)	−1.2 (1.88)	22 years	−4.8 (145)	−5.4 (48)	−8.4 (32.5)	+	+	+	severe	bicoronal and bilambdoid	AV block grade II, SN hearing loss, joint laxity, chiari I malformation, myopia
P7-1	1st	M	term	−4 (43)	−4 (30)	−2.5 (2.4)	3 years 6 months	−4.1 (83)	−5.5 (44)	−6 (8.5)	+	+	+	none	coronal, sagittal	anal stenosis, budlike mouth, ASD, VSD, undescended testes, hypospadius
P7-2	1st	F	term	−4.9 (41)	−2.9 (31)	−2.2 (2.45)	5 years 2 months	−3.5 (94)	−4 (47)	−4.2 (11.5)	+	+	+	none	coronal, sagittal	AV canal
P8	N	F	37	−0.4 (47)	−4.6 (27)	−1.7 (2.14)	4 years	−4.9 (82)	−10.4 (38.6)	−7.6 (7.5)	+ lowset	NA	+	NA	bicoronal and bilambdoid, broad patent sagittal with bifid metopic suture	vestibular, anterior anus, hearing mild conduction delay, proptosis, VSD, duodenal stenosis
P9-1	N	M	42	−1.4 (50)	NA	−1.5 (3.2)	7 years	−1.3 (115)	−2.3 (50)	−0.4 (22)	+	+	+	none	none	high arched palate, micropenis

(*Continued on next page*)

Table 2. ***Continued***

			Birth, SD				Current Exam, SD				MGS Features					
Subj.	**Consan**	**Gender**	**Gest.**	**Lgt (cm)**	**OFC (cm)**	**Wgt (kg)**	**Age**	**Hgt (cm)**	**OFC (cm)**	**Wgt (kg)**	**Microtia**	**A/Hypoplastic Patella**	**Thin Eyebrows**	**Develop. Delay**	**Craniosynostosis**	**Other Clinical Features**
P9-2	N	M	term	0.5 (52)	−1.7 (33)	−1.2 (3.0)	16 months	−2.5 (73)	−4.7 (43)	−3.7 (7.5)	+	N/A	+	none	bicoronal with widely patent metopic and sagittal sutures	none
P10	N	F	36	NA	−1.8 (30)	−1.5 (2.04)	25 years	−2.5 (149)	−4.7 (49)	NA	+	+	+	none	bicoronal	high palate, hearing loss, breast agenesis, heart block
P11	1st	F	40	NA	NA	−4.0 (1.75)	4 years 7 months	−2.5 (95)	−4.6 (−4.6)	−3.2 (12)	+	+	+	none	coronal and lambdoid	small ASD
P12-1	N	F	22+3[c]	−1.9 (25)	−3.9 (15.5)	−3.0 (0.33)	TOP				+	not reported	+	N/A	yes	anterior anus
P12-2	N	M	30+5[c]	−0.4 (39.1)	−2.9 (24)	−1.1 (1.15)	TOP				lowset	not reported	+	N/A	bicoronal, partial lambdoid, squamous and lateral parts of the occipital bone	pre-axial polydactyly of both hands, small VSD, meconium peritonitis, multiple nodules of ectopic thymic tissue, high palate

Abbreviations are as follows: NA, not available; TOP, termination of pregnancy; SD, standard deviation. Calculated using LMSgrowth[56] and adjusted for sex and gestation.
[a]Measurement at 15 years of age, after surgery.
[b]Measurement at 5 months of age.
[c]Z-scores were calculated using the Fenton 2013 Growth Calculator.[57]

In addition to craniosynostosis, clinical features variably present in individuals P1–P3 included mild short stature, microcephaly, and ear anomalies (Figure 2B, Table 2). In view of the previous association of replication-associated genes with growth restriction,[19–22] we interrogated exome-sequencing data from a cohort of individuals with primordial dwarfism (n = 52) for variants in *CDC45*. One individual (P4, family 4; II-1 in Figure 2A), diagnosed with MGS, was found to harbor two rare *CDC45* variants (Table 1).

Given the presentation of subject P4 with MGS, we then undertook dideoxy sequencing of 34 further subjects with MGS, in whom causative mutations had not previously been found in preRC components. This identified seven further families (families 5–11) (Table 1), in which nine individuals have biallelic mutations in *CDC45*. All variants had either a very low allele frequency in control populations with no homozygotes, appropriate for a rare recessively inherited Mendelian disorder, or were absent from the ExAC dataset. The autosomal-recessive inheritance was confirmed by appropriate segregation in all parents where available (Figure 2A, Table 1).

Concurrently, exome sequencing was undertaken in a nonconsanguineous Dutch family (family 12) in which two consecutive fetuses displayed craniosynostosis and additional anomalies in utero. The recurrence within the family suggested an autosomal-recessive inheritance, but no candidate disease genes were identified after bioinformatic analysis and filtering of the exome data. Given the previous findings, *CDC45* and other autosomal-recessive craniosynostosis disorder-associated genes were manually re-examined; this identified a single paternally transmitted missense variant in *CDC45*: c.893C>T encoding p.Ala298Val. Visual analysis of the sequencing reads using Integrated Genomics Viewer[29] suggested lower coverage of exon 5 in both the two affected samples and the maternal sample compared with the paternal sequencing (Figure S1A). Analysis using MLPA probes confirmed a deletion encompassing only exon 5 of *CDC45* in these three samples (Figure S1B). This would be predicted to delete a highly conserved portion of the protein, but translation would remain in-frame and therefore transcripts from this allele would not be predicted to undergo nonsense-mediated decay. This was confirmed by analysis of cDNA derived from maternal blood (Figure S1C).

The Human CDC45 Mutational Spectrum Indicates Partial Loss of Protein Function

CDC45 is an essential component in the preIC that establishes active replication at licensed origins (Figure 1). The majority of variants identified in *CDC45* lead to amino acid substitutions (Figure 3A), which bioinformatic analysis predict to be damaging; we examined conservation of these residues as a measure of deleteriousness and found all are conserved in vertebrates, with residues at several sites conserved through to yeasts (Figure 3B).

One conserved substitution, c.203A>G [p.Gln68Arg], occurred at the penultimate nucleotide in exon 3, suggesting that it might also impact splicing in addition to any protein-level consequence (see next section). The three subjects (P4, P5, P8) with a truncating/null mutation (nonsense, frameshift deletion, or initiation codon mutation) on one allele all segregate an identical missense variant, c.1388C>T [p.Pro463Leu], present on the *trans* allele; given the South Asian ancestry in all three subjects (ExAC South Asian allele frequency 0.000062), the presence of this variant is compatible with a founder effect.

All individuals had at least one allele compatible with some residual function; none were biallelic for null mutations, consistent with the early embryonic lethality reported in a *Cdc45* knockout mouse (*Cdc45* homozygotes die before E7.5, due to impaired proliferation of the inner cell mass[13]). Individuals who were compound heterozygotes for a loss-of-function and a substitution allele (those encoding p.Pro463Leu or p.Ala298Val) were particularly severely affected.

Structural Consequences of *CDC45* Mutations

Missense mutations did not cluster within a specific domain of the protein (Figure 3A). However, a homology model derived from the recent high-resolution cryo-electron microscopy study of the yeast CMG helicase complex[26] demonstrated that a number of substituted residues are located within the core of the CDC45 protein (Figures 4A and 4B). This core region corresponds to the known catalytic site of the bacterial RecJ orthologs of CDC45 and its DHH phosphoesterase homologs.[31,32] Such substitutions would therefore be likely to perturb protein stability. In particular, the recurrent p.Pro463Leu substitution replaces a conserved proline residue with a likely essential role in N-capping of an alpha helix (Figure 4C). Likewise, within the protein core, the p.Asn76His substitution is expected to introduce a positive charge within, and thus disrupt, the predicted divalent cation coordination sphere present in many members of the DHH phosphoesterase superfamily (Figure 4D).[33–35] Predictions of functional consequences for point mutations at other sites in the homology model were not possible, aside from the p.Pro321Thr substitution that is expected to disrupt the interaction of CDC45 with MCM2 (Figure 4E).

Hypomorphic *CDC45* Mutations Act by Disrupting Transcript Splicing and Reducing Protein Levels

Five of the alleles (in families 1, 3, 9, and 10) were hypothesized to affect splicing (Tables S4 and S5) and this was confirmed in the three samples available for extraction of RNA, in which we analyzed the effects of putative splicing mutations on cDNA.

In two families (families 1 and 9), the only putative second disease variants present after filtering to remove common variants were synonymous, which generally are less likely to be pathogenic. These two variants (c.318C>T

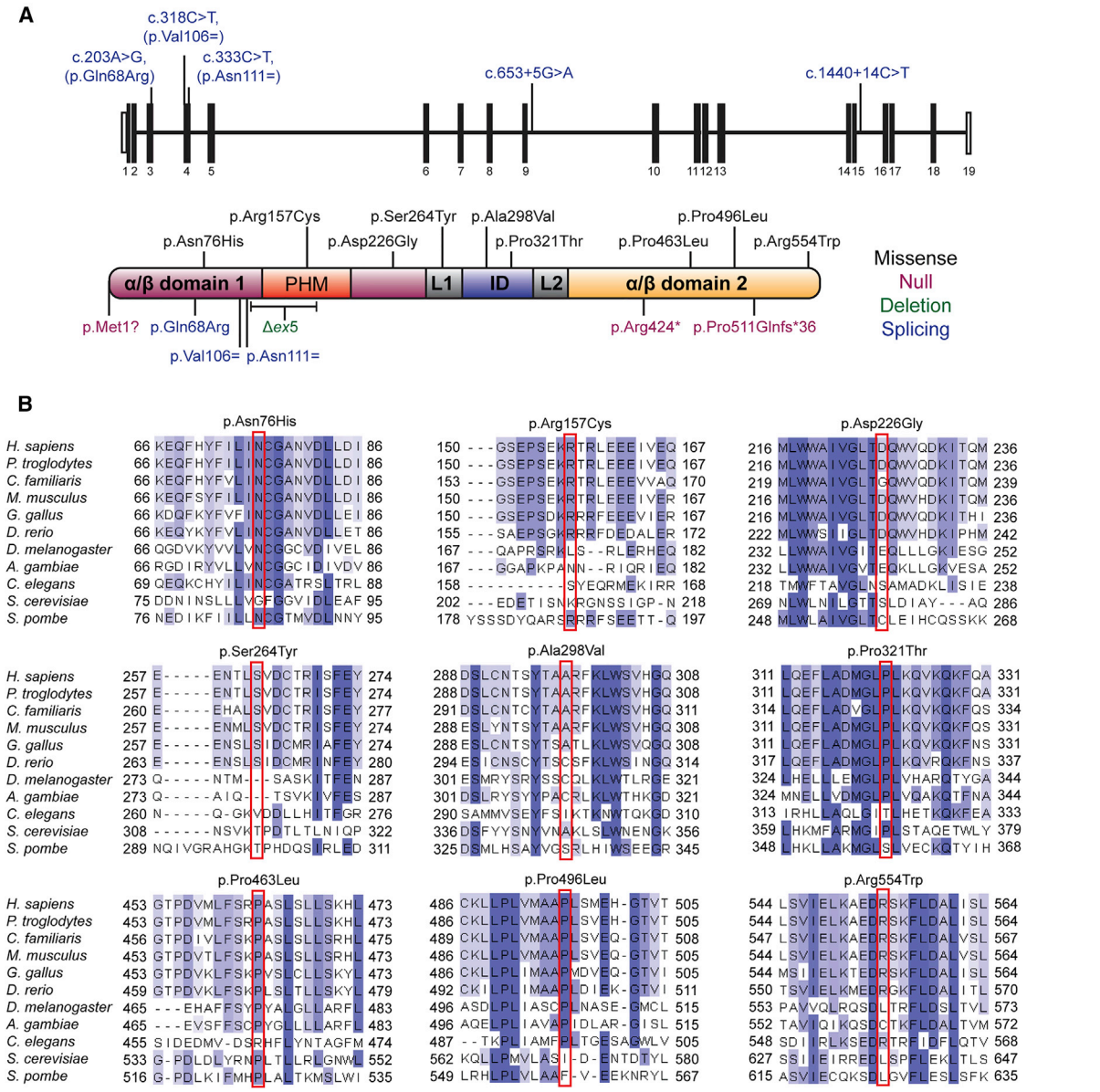

Figure 3. Mutations in CDC45 and Conservation of Substituted Residues in Orthologous Proteins

(A) Mutations identified in *CDC45* include variants predicted or shown to affect splicing (blue, position in gene shown in upper panel), predicted missense substitutions (black), or truncating mutations (purple). Δex5 refers to the intragenic deletion encompassing exon 5 of *CDC45* in family P12 (green). Mutations do not cluster within any specific domain of CDC45. Domain architecture of human CDC45 indicated as described in Yuan et al.[26] The two alpha-beta domains are shown in purple and orange, respectively. The protruding helical motif (PHM) inserted in the first alpha-beta domain is shown in red. The middle all-helix interdomain (ID) is shown in blue, and the two linkers (L1 and L2) are shown in gray.

(B) Clustal Omega alignments of eukaryotic CDC45 proteins indicate mutated residues are well conserved, with several residues (such as Asn76, Arg157, Pro321, and Pro463) conserved as distantly as fungi. Blue shading indicates proportion of conserved amino acids.

[p.Val106=] and c.333C>T [p.Asn111=]) lie close together in exon 4, which is skipped for transcripts in which alternative splicing from exon 3 directly to exon 5 generates a naturally occurring shorter isoform.[36] This evolutionarily conserved instance of exon skipping is predicted to generate an in-frame protein product that lacks part of the highly conserved DHH phosphoesterase domain.[32] RNA derived from these subjects (P1: c.318C>T, P9-1: c.333C>T) exhibited an increased ratio of exon 3/5 transcript to exon 3/4/5 cDNA product compared to control subjects (Figure 5). In silico tools (Human Splice Finder and Sroogle)[37,38] predict the c.333C>T variant to disrupt exon splice enhancer sites and the c.318C>T variant to enhance potential cryptic exonic splice silencer sites, both mechanisms by which these variants may promote the skipping of exon 4 (Table S5). The apparently nonsynonymous variant c.203A>G (mutation present in P9-1 and P9-2), which lies at the penultimate nucleotide of

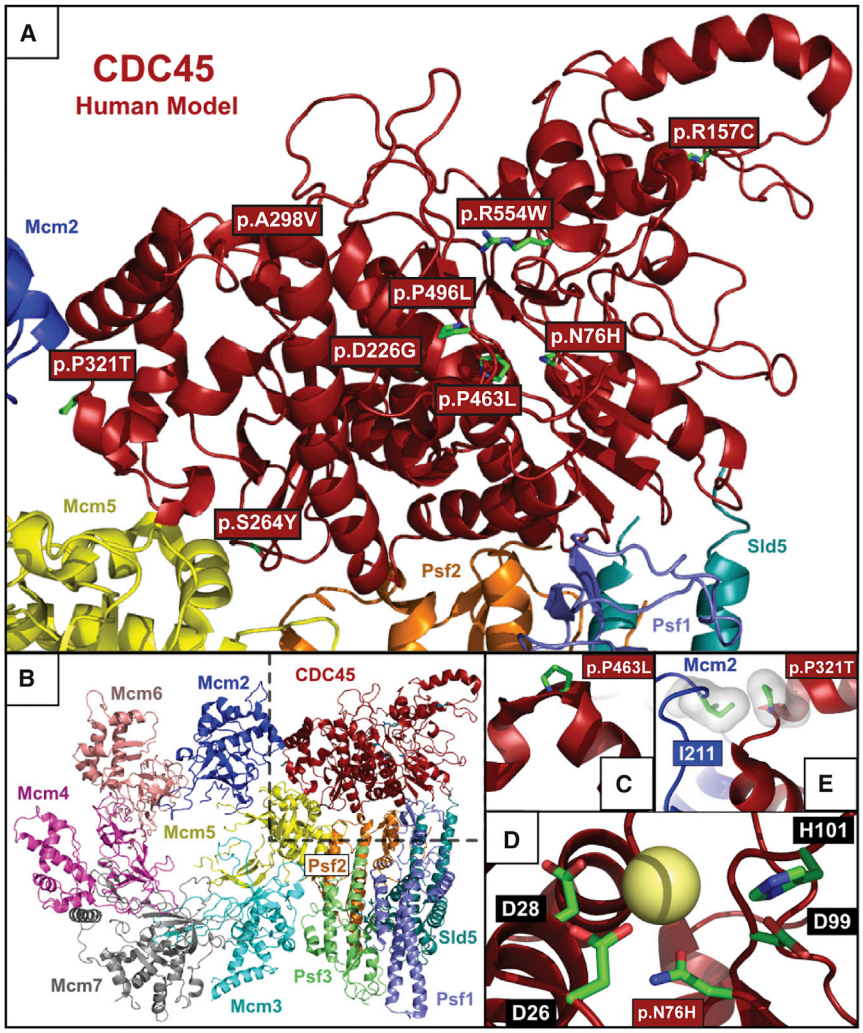

Figure 4. Structural Consequences of CDC45 Substitutions

(A) Structural model of human CDC45 demonstrating the spatial distribution of substitutions in the protein. Red boxes indicate position of missense mutations, with side chains of these substituted residues displayed in green.

(B) CDC45 in context of the *S. cerevisiae* CMG complex from the 3.8 Å cryo-electron microscopy structure.[26]

(C–E) Modeling of substitutions that cluster in the central core of CDC45.

(C) Proline 463 is an evolutionarily conserved position, with an essential role in N-capping of the alpha-helix localized between Pro542 and Cys556 in yeast Cdc45 (Pro463 and Phe477 in human). Given the location of Pro463 in the CDC45 structural core, the substitution to leucine is predicted to have severe effects on the stability of this helix[53] and therefore overall stability of the protein.

(D) Asn76 is predicted to be part of the divalent cation coordination sphere. Although the DHH domain of CDC45 is currently considered to be catalytically inert,[30,54] residues Asp26, Asp28, Asp99, and His101, corresponding to the catalytic core of prokaryotic RecJ exonucleases and the DHH superfamily of phosphoesterases, are conserved (highlighted by black boxes).[26,32,55] This suggests the continued presence of a divalent cation at this position (predicted divalent cation indicated by yellow sphere). Asn76 is therefore thought to be part of a divalent cation coordination sphere which, in other homologs, is the phosphoesterase catalytic center. The substitution to histidine would introduce a positive charge into the putative divalent cation coordination sphere, thereby disrupting the network of interactions among water molecules, charged residues and divalent cation/s observed in different members of the superfamily of DHH phosphoesterases.[33–35]

(E) Proline 321 (corresponding to Pro369 in yeast) is a key part of the CDC45 interacting surface with Mcm2,[26] given that in yeast it lies within 3.5 Å of Ile289 of Mcm2 (corresponding to Ile211 in human MCM2). Additionally, this proline has a key role in the N-capping of the alpha-helix localized between Leu370 and Gln374 in yeast Cdc45.[53] Therefore, substitution of proline 321 to threonine is likely not only to have effects on CDC45-MCM2 interaction but also on CDC45 protein stability. The interacting pair Pro321 (in CDC45) and Ile211 (corresponding to Ile289 in Mcm2) are shown in sticks (green) inside their van der Waals surfaces.

exon 3, was also shown to cause complete skipping of exon 3 in the cell line from P9-1 (Figure 5Bi).

We next sought to investigate the consequence of these mutations on the CDC45 protein by assessing protein levels in cells from five subjects by immunoblotting for endogenous CDC45 (Figure 6). In the three cell lines available from affected individuals (lymphoblastoid cell lines derived from P1, P2, and P9-1) and in primary amniocytes derived from P12-1 and P12-2, CDC45 levels were significantly lower than in multiple control cells or cell lines ($p < 0.0001$). Moreover, CDC45 levels were reduced below 50% in all cases, indicating a contribution from both alleles to reduced protein levels. This suggests that the missense variants present in these cells or cell lines (P1, p.Asp226Gly; P2, p.Asn76His and p.Arg157Cys; P12, p.Ala298Val) each result in destabilization of CDC45 protein.

Taken together with the nature of the mutations identified, the key demonstration of decreased cellular levels in several affected individuals confirm that variants identified were pathogenic and the mutations would most likely result in destabilization of CDC45 protein.

Spectrum of Phenotypes Associated with *CDC45* Mutations and Correlation with Genotype

In total we identified 15 subjects from 12 families with variants in *CDC45* (Table 1, Figure 2A). Individuals with biallelic *CDC45* mutations exhibit substantial variation in severity, in part explained by ascertainment from two distinct cohorts of affected subjects (craniosynostosis for P1–P3 and P12 and MGS for P4–P11). Nevertheless they manifest a recognizable phenotypic spectrum with overlapping clinical features (Table 2, Figures 2B–2D).

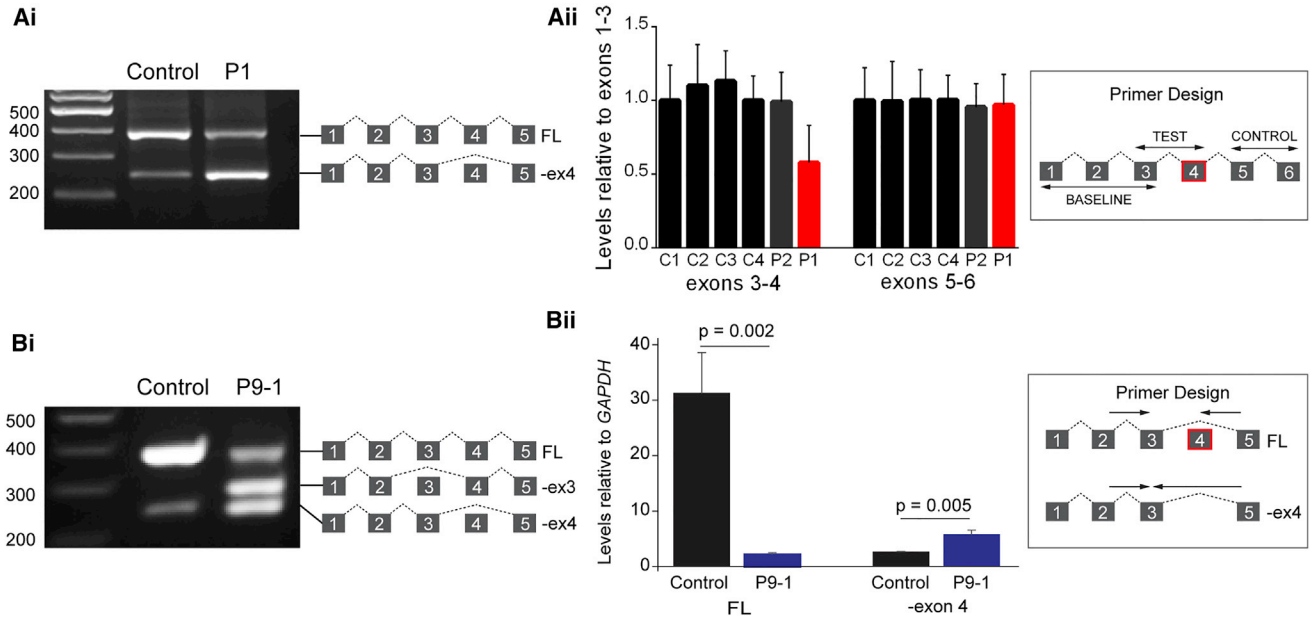

Figure 5. Synonymous *CDC45* Variants Alter Levels of Alternative Splicing of Exon 4 in Lymphoblastoid Cell Lines
(A) The synonymous variant c.318C>T present in P1 increases the ratio of exon3/5 transcript compared to controls. (i) RT-PCR demonstrating an enrichment in the exon3/5 lower band. (ii) Results of qRT-PCR to assay the relative amounts of exon 4 in P1, P2, and four unaffected control subjects. Products were amplified with primers in exons 3 and 4 and compared with products generated from primers in exons 1 and 3. cDNA from P1 showed a 0.43-fold reduction in exons 3–4 relative to exons 1–3. Levels of exons 5–6 compared with exons 1–3 are also shown, no differences were observed. Error bars, standard deviation. n = 3 experimental replicates of qPCR.
(B) The synonymous variant c.333C>T together with the *trans* c.203A>G (p.Glu68Arg) splice site variant identified in P9-1 and P9-2 increases aberrant splicing across this region of the gene. (i) RT-PCR demonstrating an increase in exon3/5 transcript and the creation of a novel transcript where exon 3 has been skipped due to the c.203A>G mutation. (ii) Total RNA extracted from LCLs derived from P9-1 was analyzed by qRT-PCR. Full-length-only transcripts were amplified using a forward primer (F 2/3) spanning the exon 2-exon 3 boundary and a reverse primer (R 4/5) spanning the exon 4-exon 5 boundary. The transcript missing exon 4 was specifically amplified using the F 2/3 primer paired with a reverse primer (R 3/5) which spanned the exon 3-exon 5 boundary. Total amount of minus exon 4 (−Ex4) and full-length (FL) transcript was normalized to *GAPDH* for P9-1 and control. Error bars indicate standard deviation (n = 3 experiments). A two-tailed, unpaired Student's t test was performed and p values are indicated.

For example, although subjects P4–P11 all presented with the classical triad of MGS features (short stature from −1.3 to −7.7 SD, microtia, and absent or hypoplastic patellae), craniosynostosis was also frequent, in contrast to MGS associated with mutations in preRC components. The severity of craniosynostosis varied widely from unilateral or bilateral coronal synostosis to multiple suture involvement (Figure 2C). The discordance for craniosynostosis in two siblings with identical mutations (P9-1 and P9-2) indicates that this is not a fully penetrant phenotype. Conversely, individuals with a primary presentation of craniosynostosis also exhibited mild MGS features, such as hypoplastic ears (P1, P3, P12-1), mild short stature, and a similar facial gestalt including a small mouth (Figure 2B). The MGS feature of patellar hypoplasia was, however, not observed in any of the three individuals with craniosynostosis who presented postnatally (P1–P3). Thin eyebrows were present in subjects presenting with either craniosynostosis or MGS, a feature that has not been previously highlighted in these or related developmental disorders. Additionally, anal abnormalities (imperforate anus or anterior placement) were present in seven subjects drawn from both cohorts. Growth failure and microcephaly were evident from birth in almost all subjects (Figure 2D), and both the microcephaly and height reduction were progressive throughout childhood. Carrier parents and heterozygous siblings were phenotypically normal, a point of particular note since *CDC45* is located on 22q11.21, within the interval deleted in the 22q11.2 deletion syndromes.[39]

Discussion

Here we identify multiple mutations in *CDC45*, implicating its involvement in the pathogenesis of both MGS and craniosynostosis. Previous work had established MGS as a disorder of replication licensing, with biallelic mutations in *ORC1*, *ORC4*, and *ORC6* and accessory proteins encoded by *CDC6* and *CDT1*. Furthermore, a recent report has identified stabilizing mutations in *GMNN*, which probably act to inhibit CDT1 and consequently reduce licensing in G_1.[23] No mutations in any of the MCM subunits have been discovered in individuals with MGS, previously suggesting that MGS was limited to the upstream preRC components; indeed, a founder *MCM4* mutation has been described causing a distinct entity—a genome instability syndrome of short stature, adrenal insufficiency, and primary immunodeficiency.[40–42] The identification of

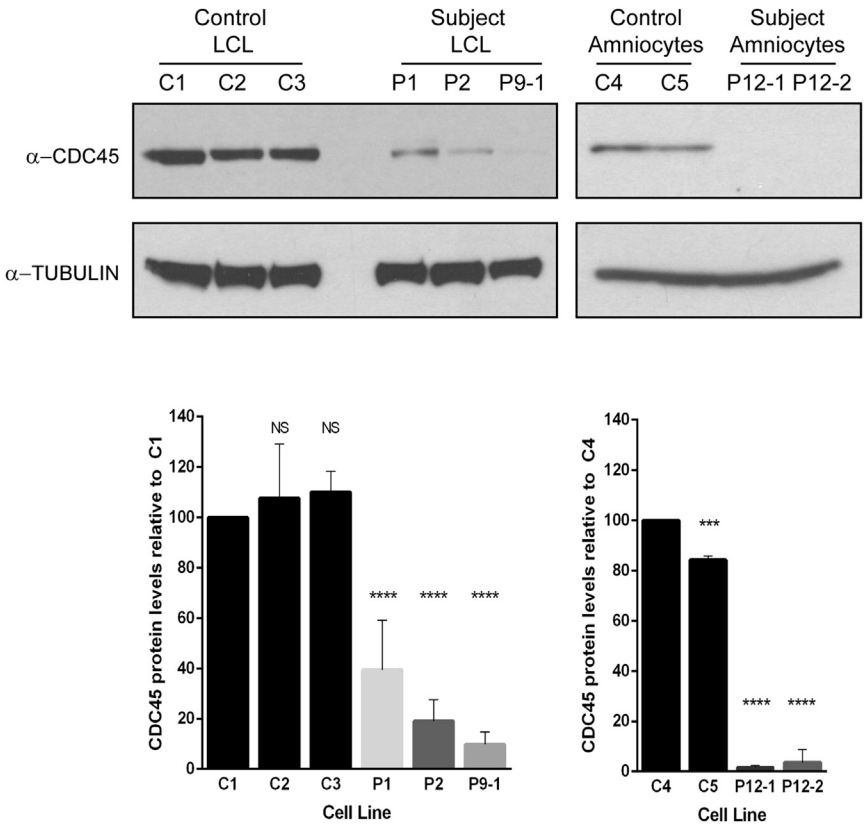

Figure 6. CDC45 Protein Levels Are Significantly Reduced in Lymphoblastoid Cell Lines and Primary Amniocytes

Cell lines from affected individuals (P1, P2, P9-1) and amniocytes derived from affected fetuses (P12-1 and P12-2) demonstrate a significant reduction in endogenous CDC45 levels compared to three independent controls (LCL samples: one-way ANOVA comparing all LCL samples against C1; error bars indicate standard deviation; NS, $p > 0.01$, ****$p < 0.0001$, $n = 5$ biological replicates; amniocyte samples: one-way ANOVA comparing all amniocyte samples against C4. ***$p < 0.001$, ****$p < 0.0001$, $n = 3$ biological replicates).

CDC45 is therefore surprising, given the well-established function of CDC45 in replication activation and fork progression (Figure 1). Associating *CDC45* mutations with MGS therefore expands understanding of the pathogenic basis of MGS, and given the number of individuals reported here, establishes *CDC45* as a common cause of MGS syndrome, alongside *ORC1* and *CDT1*. These mutations in individuals with MGS also raise the possibility that mutations in genes coding for other proteins involved in DNA replication may be implicated in MGS and/or craniosynostosis.[17,43–45]

After the initial identification of MGS mutations, several studies have proposed disease mechanisms distinct from the canonical role of the preRC in replication, such as dysregulated cilia formation or centrosome duplication.[46,47] Our identification of MGS mutations in distinct replication machinery, with similar growth and clinical characteristics seen in the preRC MGS-affected individuals (including those with *GMNN* mutations), strongly favors a replication-based etiology for MGS. Notably, biallelic mutations in the helicase *RECQL4* (MIM: 603780, also required for preIC formation and replication initiation[44,45]) can cause a phenotype that overlaps with MGS; RAPADILINO syndrome (MIM: 266280) is characterized by growth retardation and patellar agenesis, although diarrhea, palatal anomalies, and radial ray defects are also evident.[45] Since CDC45 has been shown to bind several additional proteins in the preIC, for example TOPBP1[48] and MCM10,[49] mutations of these other components may in future be implicated in MGS or disorders exhibiting overlapping features.

A distinctive feature of MGS caused by *CDC45* mutations is the frequent association with craniosynostosis. Only one previous MGS-affected subject, harboring mutations in *ORC1*, has been reported with craniosynostosis (P1 in Bicknell et al.[20]); therefore, it is likely that the presence of craniosynostosis in MGS-affected subjects is a strong predictor for *CDC45* mutations. Craniosynostosis is also a feature of Baller-Gerold syndrome (MIM: 218600), another *RECQL4* disorder,[45] further implicating replication initiation in the etiology of premature cranial suture closure.

Disruption of the canonical function of CDC45 in replication initiation is consistent with the previously proposed models to explain the growth phenotype, which suggested that impaired replication in affected individuals disrupts cell division during periods of rapid proliferation in development, ultimately impairing organism growth and leading to a "hypocellular" dwarfism.[20,50] Partial loss-of-function mutations in *CDC45*, like those in preRC components, further indicate that strict regulation of replication is particularly required for the development of specific cartilaginous structures (ear, patella, trachea, or bronchial tree),[51] but the exact mechanism remains elusive and future studies with model organisms will be required. Similarly, the frequent occurrence of craniosynostosis in this cohort, along with the established premature suture fusion seen in subjects with *RECQL4* mutations, highlights the importance of normal replication initiation and progression to maintain correct proliferation-differentiation balance in the cranial sutures.[52]

In summary, we present genetic and functional evidence that mutations in *CDC45* cause Meier-Gorlin syndrome with craniosynostosis. The identification of these mutations in a DNA replication protein functioning downstream to the previously identified MGS genes reinforces the premise that the growth and cartilaginous phenotypes

of MGS, as well as the premature cranial suture fusion seen here, are due to replication dysfunction. This identification also suggests new candidate genes in which mutations might underlie this disorder or component phenotypes.

Supplemental Data

Supplemental Data include Supplementary Notes, Tables S1–S5, and Figure S1 and can be found with this article online at http://dx.doi.org/10.1016/j.ajhg.2016.05.019.

Acknowledgments

We thank the families and clinicians for their participation, the IGMM core sequencing service, staff at the High-Throughput Genomics facility at the Wellcome Trust Centre for Human Genetics (Oxford) for Illumina sequencing, Tim Forshew and Francesco Marass for primer design, and Sue Butler, John Frankland, and Tim Rostron for help with cell culture and DNA sequencing. This work was supported by funding from the Medical Research Council (MRC) (A.P.J., L.S.-P., C.P.P., W.N.) and through the WIMM Strategic Alliance (G0902418 and MC_UU_12025), the European Research Council (ERC, 281847) (A.P.J.), the Lister Institute for Preventative Medicine (A.P.J.), Medical Research Scotland (L.S.B.), Royal Society of New Zealand Rutherford Discovery Fellowship (L.S.B.), the Department of Health, UK, Quality, Improvement, Development and Initiative Scheme (QIDIS) (A.O.M.W.), Newlife Foundation for Disabled Children (SG/14-15/10 to A.O.M.W.), National Institute for Health Research (NIHR) Oxford Biomedical Research Centre Programme (A.O.M.W.), and the Wellcome Trust (Project Grant 093329 to A.O.M.W. and S.R.F.T.; Investigator Award 102731 to A.O.M.W.).

Received: March 30, 2016
Accepted: May 9, 2016
Published: June 30, 2016

Web Resources

1000 Genomes, http://www.1000genomes.org
dbSNP, http://www.ncbi.nlm.nih.gov/projects/SNP/
ExAC Browser, http://exac.broadinstitute.org/
GoNL (Genomes of the Netherlands), http://www.nlgenome.nl/search/
NHLBI Exome Sequencing Project (ESP) Exome Variant Server, http://evs.gs.washington.edu/EVS/
OMIM, http://www.omim.org/
PyMOL, http://www.pymol.org
RefSeq, http://www.ncbi.nlm.nih.gov/RefSeq

References

1. Bell, S.P., and Stillman, B. (1992). ATP-dependent recognition of eukaryotic origins of DNA replication by a multiprotein complex. Nature *357*, 128–134.
2. Tanaka, S., and Diffley, J.F. (2002). Interdependent nuclear accumulation of budding yeast Cdt1 and Mcm2-7 during G1 phase. Nat. Cell Biol. *4*, 198–207.
3. Tanaka, S., and Araki, H. (2013). Helicase activation and establishment of replication forks at chromosomal origins of replication. Cold Spring Harb. Perspect. Biol. *5*, a010371.
4. Costa, A., Renault, L., Swuec, P., Petojevic, T., Pesavento, J.J., Ilves, I., MacLellan-Gibson, K., Fleck, R.A., Botchan, M.R., and Berger, J.M. (2014). DNA binding polarity, dimerization, and ATPase ring remodeling in the CMG helicase of the eukaryotic replisome. eLife *3*, e03273.
5. Ilves, I., Petojevic, T., Pesavento, J.J., and Botchan, M.R. (2010). Activation of the MCM2-7 helicase by association with Cdc45 and GINS proteins. Mol. Cell *37*, 247–258.
6. Li, N., Zhai, Y., Zhang, Y., Li, W., Yang, M., Lei, J., Tye, B.K., and Gao, N. (2015). Structure of the eukaryotic MCM complex at 3.8 Å. Nature *524*, 186–191.
7. Moyer, S.E., Lewis, P.W., and Botchan, M.R. (2006). Isolation of the Cdc45/Mcm2-7/GINS (CMG) complex, a candidate for the eukaryotic DNA replication fork helicase. Proc. Natl. Acad. Sci. USA *103*, 10236–10241.
8. Pacek, M., Tutter, A.V., Kubota, Y., Takisawa, H., and Walter, J.C. (2006). Localization of MCM2-7, Cdc45, and GINS to the site of DNA unwinding during eukaryotic DNA replication. Mol. Cell *21*, 581–587.
9. Szambowska, A., Tessmer, I., Kursula, P., Usskilat, C., Prus, P., Pospiech, H., and Grosse, F. (2014). DNA binding properties of human Cdc45 suggest a function as molecular wedge for DNA unwinding. Nucleic Acids Res. *42*, 2308–2319.
10. Hopwood, B., and Dalton, S. (1996). Cdc45p assembles into a complex with Cdc46p/Mcm5p, is required for minichromosome maintenance, and is essential for chromosomal DNA replication. Proc. Natl. Acad. Sci. USA *93*, 12309–12314.
11. Mimura, S., and Takisawa, H. (1998). Xenopus Cdc45-dependent loading of DNA polymerase alpha onto chromatin under the control of S-phase Cdk. EMBO J. *17*, 5699–5707.
12. Miyake, S., and Yamashita, S. (1998). Identification of sna41 gene, which is the suppressor of nda4 mutation and is involved in DNA replication in *Schizosaccharomyces pombe*. Genes Cells *3*, 157–166.
13. Yoshida, K., Kuo, F., George, E.L., Sharpe, A.H., and Dutta, A. (2001). Requirement of CDC45 for postimplantation mouse development. Mol. Cell. Biol. *21*, 4598–4603.
14. Zou, L., Mitchell, J., and Stillman, B. (1997). CDC45, a novel yeast gene that functions with the origin recognition complex and Mcm proteins in initiation of DNA replication. Mol. Cell. Biol. *17*, 553–563.
15. Heller, R.C., Kang, S., Lam, W.M., Chen, S., Chan, C.S., and Bell, S.P. (2011). Eukaryotic origin-dependent DNA replication in vitro reveals sequential action of DDK and S-CDK kinases. Cell *146*, 80–91.
16. On, K.F., Beuron, F., Frith, D., Snijders, A.P., Morris, E.P., and Diffley, J.F. (2014). Prereplicative complexes assembled in vitro support origin-dependent and independent DNA replication. EMBO J. *33*, 605–620.
17. Yeeles, J.T., Deegan, T.D., Janska, A., Early, A., and Diffley, J.F. (2015). Regulated eukaryotic DNA replication origin firing with purified proteins. Nature *519*, 431–435.
18. Bongers, E.M., Opitz, J.M., Fryer, A., Sarda, P., Hennekam, R.C., Hall, B.D., Superneau, D.W., Harbison, M., Poss, A., van Bokhoven, H., et al. (2001). Meier-Gorlin syndrome: report of

eight additional cases and review. Am. J. Med. Genet. *102*, 115–124.
19. Bicknell, L.S., Bongers, E.M., Leitch, A., Brown, S., Schoots, J., Harley, M.E., Aftimos, S., Al-Aama, J.Y., Bober, M., Brown, P.A., et al. (2011). Mutations in the pre-replication complex cause Meier-Gorlin syndrome. Nat. Genet. *43*, 356–359.
20. Bicknell, L.S., Walker, S., Klingseisen, A., Stiff, T., Leitch, A., Kerzendorfer, C., Martin, C.A., Yeyati, P., Al Sanna, N., Bober, M., et al. (2011). Mutations in ORC1, encoding the largest subunit of the origin recognition complex, cause microcephalic primordial dwarfism resembling Meier-Gorlin syndrome. Nat. Genet. *43*, 350–355.
21. Guernsey, D.L., Matsuoka, M., Jiang, H., Evans, S., Macgillivray, C., Nightingale, M., Perry, S., Ferguson, M., LeBlanc, M., Paquette, J., et al. (2011). Mutations in origin recognition complex gene ORC4 cause Meier-Gorlin syndrome. Nat. Genet. *43*, 360–364.
22. de Munnik, S.A., Hoefsloot, E.H., Roukema, J., Schoots, J., Knoers, N.V., Brunner, H.G., Jackson, A.P., and Bongers, E.M. (2015). Meier-Gorlin syndrome. Orphanet J. Rare Dis. *10*, 114.
23. Burrage, L.C., Charng, W.L., Eldomery, M.K., Willer, J.R., Davis, E.E., Lugtenberg, D., Zhu, W., Leduc, M.S., Akdemir, Z.C., Azamian, M., et al. (2015). De novo GMNN mutations cause autosomal-dominant primordial dwarfism associated with Meier-Gorlin syndrome. Am. J. Hum. Genet. *97*, 904–913.
24. Yoshida, K., Oyaizu, N., Dutta, A., and Inoue, I. (2004). The destruction box of human Geminin is critical for proliferation and tumor growth in human colon cancer cells. Oncogene *23*, 58–70.
25. Sievers, F., Wilm, A., Dineen, D., Gibson, T.J., Karplus, K., Li, W., Lopez, R., McWilliam, H., Remmert, M., Söding, J., et al. (2011). Fast, scalable generation of high-quality protein multiple sequence alignments using Clustal Omega. Mol. Syst. Biol. *7*, 539.
26. Yuan, Z., Bai, L., Sun, J., Georgescu, R., Liu, J., O'Donnell, M.E., and Li, H. (2016). Structure of the eukaryotic replicative CMG helicase suggests a pumpjack motion for translocation. Nat. Struct. Mol. Biol. *23*, 217–224.
27. Sali, A., and Blundell, T.L. (1993). Comparative protein modelling by satisfaction of spatial restraints. J. Mol. Biol. *234*, 779–815.
28. Taylor, J.C., Martin, H.C., Lise, S., Broxholme, J., Cazier, J.B., Rimmer, A., Kanapin, A., Lunter, G., Fiddy, S., Allan, C., et al. (2015). Factors influencing success of clinical genome sequencing across a broad spectrum of disorders. Nat. Genet. *47*, 717–726.
29. Robinson, J.T., Thorvaldsdóttir, H., Winckler, W., Guttman, M., Lander, E.S., Getz, G., and Mesirov, J.P. (2011). Integrative genomics viewer. Nat. Biotechnol. *29*, 24–26.
30. Abid Ali, F., Renault, L., Gannon, J., Gahlon, H.L., Kotecha, A., Zhou, J.C., Rueda, D., and Costa, A. (2016). Cryo-EM structures of the eukaryotic replicative helicase bound to a translocation substrate. Nat. Commun. *7*, 10708.
31. Krastanova, I., Sannino, V., Amenitsch, H., Gileadi, O., Pisani, F.M., and Onesti, S. (2012). Structural and functional insights into the DNA replication factor Cdc45 reveal an evolutionary relationship to the DHH family of phosphoesterases. J. Biol. Chem. *287*, 4121–4128.
32. Sanchez-Pulido, L., and Ponting, C.P. (2011). Cdc45: the missing RecJ ortholog in eukaryotes? Bioinformatics *27*, 1885–1888.
33. He, Q., Wang, F., Liu, S., Zhu, D., Cong, H., Gao, F., Li, B., Wang, H., Lin, Z., Liao, J., and Gu, L. (2016). Structural and biochemical insight into the mechanism of Rv2837c from *Mycobacterium tuberculosis* as a c-di-NMP phosphodiesterase. J. Biol. Chem. *291*, 3668–3681.
34. Wakamatsu, T., Kim, K., Uemura, Y., Nakagawa, N., Kuramitsu, S., and Masui, R. (2011). Role of RecJ-like protein with 5′-3′ exonuclease activity in oligo(deoxy)nucleotide degradation. J. Biol. Chem. *286*, 2807–2816.
35. Yamagata, A., Kakuta, Y., Masui, R., and Fukuyama, K. (2002). The crystal structure of exonuclease RecJ bound to Mn2+ ion suggests how its characteristic motifs are involved in exonuclease activity. Proc. Natl. Acad. Sci. USA *99*, 5908–5912.
36. Kukimoto, I., Igaki, H., and Kanda, T. (1999). Human CDC45 protein binds to minichromosome maintenance 7 protein and the p70 subunit of DNA polymerase alpha. Eur. J. Biochem. *265*, 936–943.
37. Desmet, F.O., Hamroun, D., Lalande, M., Collod-Béroud, G., Claustres, M., and Béroud, C. (2009). Human Splicing Finder: an online bioinformatics tool to predict splicing signals. Nucleic Acids Res. *37*, e67.
38. Schwartz, S., Hall, E., and Ast, G. (2009). SROOGLE: webserver for integrative, user-friendly visualization of splicing signals. Nucleic Acids Res. *37*, W189–W192.
39. Delio, M., Guo, T., McDonald-McGinn, D.M., Zackai, E., Herman, S., Kaminetzky, M., Higgins, A.M., Coleman, K., Chow, C., Jalbrzikowski, M., et al. (2013). Enhanced maternal origin of the 22q11.2 deletion in velocardiofacial and DiGeorge syndromes. Am. J. Hum. Genet. *92*, 439–447.
40. Casey, J.P., Nobbs, M., McGettigan, P., Lynch, S., and Ennis, S. (2012). Recessive mutations in MCM4/PRKDC cause a novel syndrome involving a primary immunodeficiency and a disorder of DNA repair. J. Med. Genet. *49*, 242–245.
41. Gineau, L., Cognet, C., Kara, N., Lach, F.P., Dunne, J., Veturi, U., Picard, C., Trouillet, C., Eidenschenk, C., Aoufouchi, S., et al. (2012). Partial MCM4 deficiency in patients with growth retardation, adrenal insufficiency, and natural killer cell deficiency. J. Clin. Invest. *122*, 821–832.
42. Hughes, C.R., Guasti, L., Meimaridou, E., Chuang, C.H., Schimenti, J.C., King, P.J., Costigan, C., Clark, A.J., and Metherell, L.A. (2012). MCM4 mutation causes adrenal failure, short stature, and natural killer cell deficiency in humans. J. Clin. Invest. *122*, 814–820.
43. Im, J.S., Ki, S.H., Farina, A., Jung, D.S., Hurwitz, J., and Lee, J.K. (2009). Assembly of the Cdc45-Mcm2-7-GINS complex in human cells requires the Ctf4/And-1, RecQL4, and Mcm10 proteins. Proc. Natl. Acad. Sci. USA *106*, 15628–15632.
44. Sangrithi, M.N., Bernal, J.A., Madine, M., Philpott, A., Lee, J., Dunphy, W.G., and Venkitaraman, A.R. (2005). Initiation of DNA replication requires the RECQL4 protein mutated in Rothmund-Thomson syndrome. Cell *121*, 887–898.
45. Siitonen, H.A., Sotkasiira, J., Biervliet, M., Benmansour, A., Capri, Y., Cormier-Daire, V., Crandall, B., Hannula-Jouppi, K., Hennekam, R., Herzog, D., et al. (2009). The mutation spectrum in RECQL4 diseases. Eur. J. Hum. Genet. *17*, 151–158.
46. Hossain, M., and Stillman, B. (2012). Meier-Gorlin syndrome mutations disrupt an Orc1 CDK inhibitory domain and cause centrosome reduplication. Genes Dev. *26*, 1797–1810.

47. Stiff, T., Alagoz, M., Alcantara, D., Outwin, E., Brunner, H.G., Bongers, E.M., O'Driscoll, M., and Jeggo, P.A. (2013). Deficiency in origin licensing proteins impairs cilia formation: implications for the aetiology of Meier-Gorlin syndrome. PLoS Genet. *9*, e1003360.
48. Schmidt, U., Wollmann, Y., Franke, C., Grosse, F., Saluz, H.P., and Hänel, F. (2008). Characterization of the interaction between the human DNA topoisomerase IIbeta-binding protein 1 (TopBP1) and the cell division cycle 45 (Cdc45) protein. Biochem. J. *409*, 169–177.
49. Di Perna, R., Aria, V., De Falco, M., Sannino, V., Okorokov, A.L., Pisani, F.M., and De Felice, M. (2013). The physical interaction of Mcm10 with Cdc45 modulates their DNA-binding properties. Biochem. J. *454*, 333–343.
50. Klingseisen, A., and Jackson, A.P. (2011). Mechanisms and pathways of growth failure in primordial dwarfism. Genes Dev. *25*, 2011–2024.
51. de Munnik, S.A., Bicknell, L.S., Aftimos, S., Al-Aama, J.Y., van Bever, Y., Bober, M.B., Clayton-Smith, J., Edrees, A.Y., Feingold, M., Fryer, A., et al. (2012). Meier-Gorlin syndrome genotype-phenotype studies: 35 individuals with pre-replication complex gene mutations and 10 without molecular diagnosis. Eur. J. Hum. Genet. *20*, 598–606.
52. Twigg, S.R.F., and Wilkie, A.O.M. (2015). A genetic-pathophysiological framework for craniosynostosis. Am. J. Hum. Genet. *97*, 359–377.
53. Newell, N.E. (2015). Mapping side chain interactions at protein helix termini. BMC Bioinformatics *16*, 231.
54. Berti, M., and Vindigni, A. (2016). Replication stress: getting back on track. Nat. Struct. Mol. Biol. *23*, 103–109.
55. Aravind, L., and Koonin, E.V. (1998). The HD domain defines a new superfamily of metal-dependent phosphohydrolases. Trends Biochem. Sci. *23*, 469–472.
56. Cole, T.J., Freeman, J.V., and Preece, M.A. (1998). British 1990 growth reference centiles for weight, height, body mass index and head circumference fitted by maximum penalized likelihood. Stat. Med. *17*, 407–429.
57. Fenton, T.R., and Kim, J.H. (2013). A systematic review and meta-analysis to revise the Fenton growth chart for preterm infants. BMC Pediatr. *13*, 59.

The American Journal of Human Genetics, Volume *99*

Supplemental Data

Mutations in *CDC45*, Encoding an Essential Component of the Pre-initiation Complex, Cause Meier-Gorlin Syndrome and Craniosynostosis

Aimee L. Fenwick, Maciej Kliszczak, Fay Cooper, Jennie Murray, Luis Sanchez-Pulido, Stephen R.F. Twigg, Anne Goriely, Simon J. McGowan, Kerry A. Miller, Indira B. Taylor, Clare Logan, WGS500 Consortium, Sevcan Bozdogan, Sumita Danda, Joanne Dixon, Solaf M. Elsayed, Ezzat Elsobky, Alice Gardham, Mariette J.V. Hoffer, Marije Koopmans, Donna M. McDonald-McGinn, Gijs W.E. Santen, Ravi Savarirayan, Deepthi de Silva, Olivier Vanakker, Steven A. Wall, Louise C. Wilson, Ozge Ozalp Yuregir, Elaine H. Zackai, Chris P. Ponting, Andrew P. Jackson, Andrew O.M. Wilkie, Wojciech Niedzwiedz, and Louise S. Bicknell

Supplementary Note.

WGS500: names and affiliations of authors

Steering Committee: Peter Donnelly (Chair)[1], John Bell[2], David Bentley[3], Gil McVean[1], Peter Ratcliffe[1], Jenny Taylor[1,4], Andrew Wilkie[4,5]

Operations Committee: Peter Donnelly (Chair)[1], John Broxholme[1], David Buck[1], Jean-Baptiste Cazier[1], Richard Cornall[1], Lorna Gregory[1], Julian Knight[1], Gerton Lunter[1], Gil McVean[1], Jenny Taylor[1,4], Ian Tomlinson[1,4], Andrew Wilkie[4,5]

Sequencing & Experimental Follow up: David Buck (Lead)[1], Christopher Allan[1], Moustafa Attar[1], Angie Green[1], Lorna Gregory[1], Sean Humphray[3], Zoya Kingsbury[3], Sarah Lamble[1], Lorne Lonie[1], Alistair Pagnamenta[1], Paolo Piazza[1], Guadelupe Polanco[1], Amy Trebes[1]

Data Analysis: Gil McVean[1] (Lead), Peter Donnelly[1], Jean-Baptiste Cazier[1], John Broxholme[1], Richard Copley[1], Simon Fiddy[1], Russell Grocock[3], Edouard Hatton[1], Chris Holmes[1], Linda Hughes[1], Peter Humburg[1], Alexander Kanapin[1], Stefano Lise[1], Gerton Lunter[1], Hilary Martin[1], Lisa Murray[3], Davis McCarthy[1], Andy Rimmer[1], Natasha Sahgal[1], Ben Wright[1], Chris Yau[6]

[1]The Wellcome Trust Centre for Human Genetics, Roosevelt Drive, Oxford, OX3 7BN, UK

[2]Office of the Regius Professor of Medicine, Richard Doll Building, Roosevelt Drive, Oxford, OX3 7LF, UK

[3]Illumina Cambridge Ltd., Chesterford Research Park, Little Chesterford, Essex, CB10 1XL, UK

[4]NIHR Oxford Biomedical Research Centre, Oxford, UK

[5]Weatherall Institute of Molecular Medicine, John Radcliffe Hospital, Headington, Oxford OX3 9DS, UK

[6]Imperial College London, South Kensington Campus, London, SW7 2AZ, UK

Note on accession numbers for *CDC45*

Human *CDC45* encodes a 20-exon gene that has been annotated as including three major spliceforms. As well as the full-length version which encodes a protein of 598 amino acids, alternative splicing to skip either exon 7 alone or both exons 4 and 7 leads to shorter isoforms with in-frame deletions of 32 and 78 amino acids, respectively. Whereas exon 4 shows high conservation in mammalian species both in sequence and occurrence of exon skipping, neither is the case for exon 7, so the physiological significance of the isoform including exon 7 is currently uncertain. Virtually all previous publications investigating the structure and function of CDC45 employ the numbering of the middle-sized, 566 amino acid isoform, so for consistency with prior work all numbering used here refers to NM_003504.4.

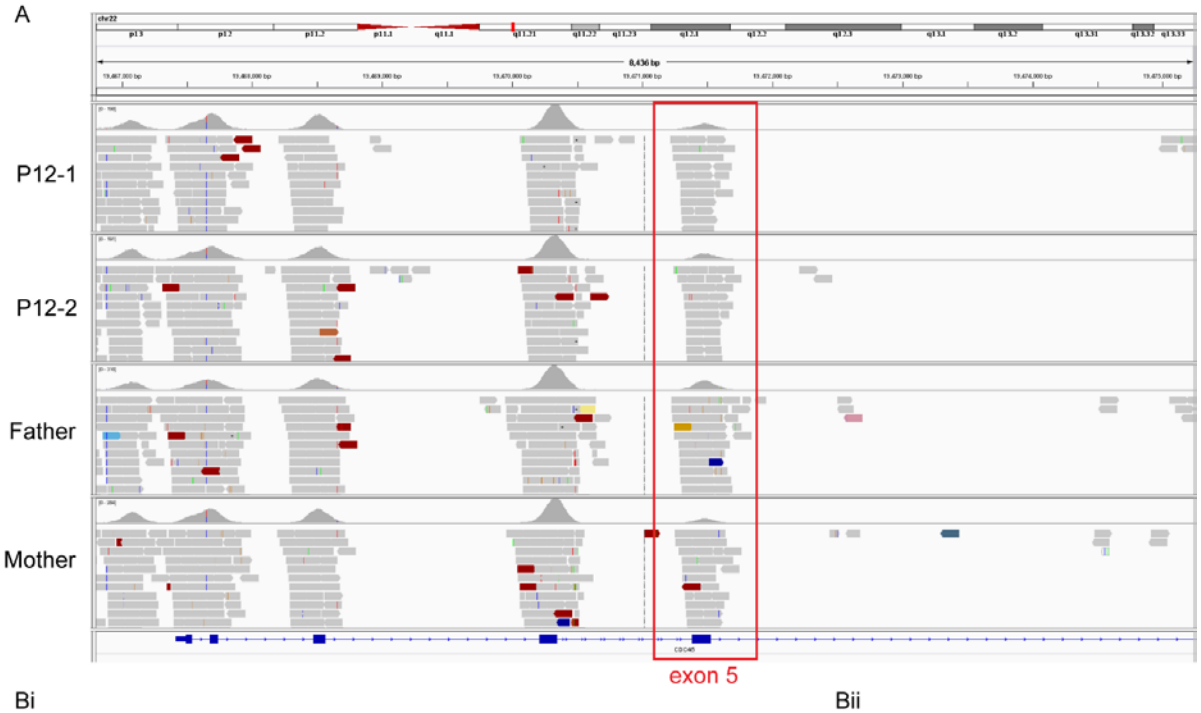

Bi

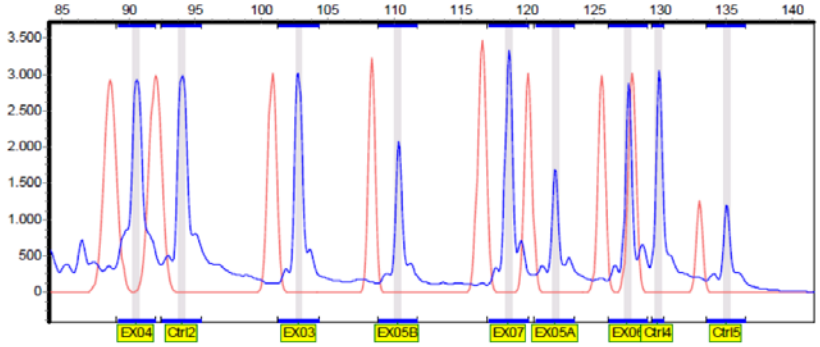

Bii

Probe Number	MLPA Ratio vs Control
Ctrl2	0.998
Ctrl4	1.008
Ctrl5	0.948
EX03	0.999
EX04	1.002
EX05A	0.561
EX05B	0.643
EX06	0.959
EX07	0.962

Ci

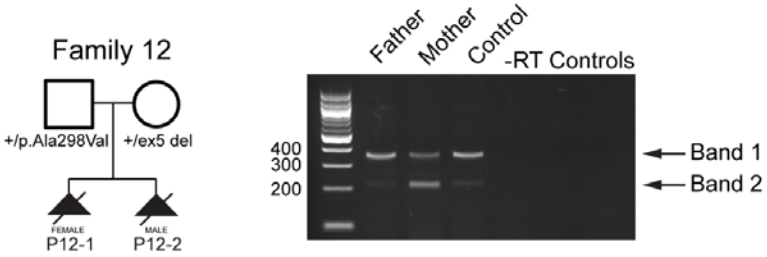

Cii

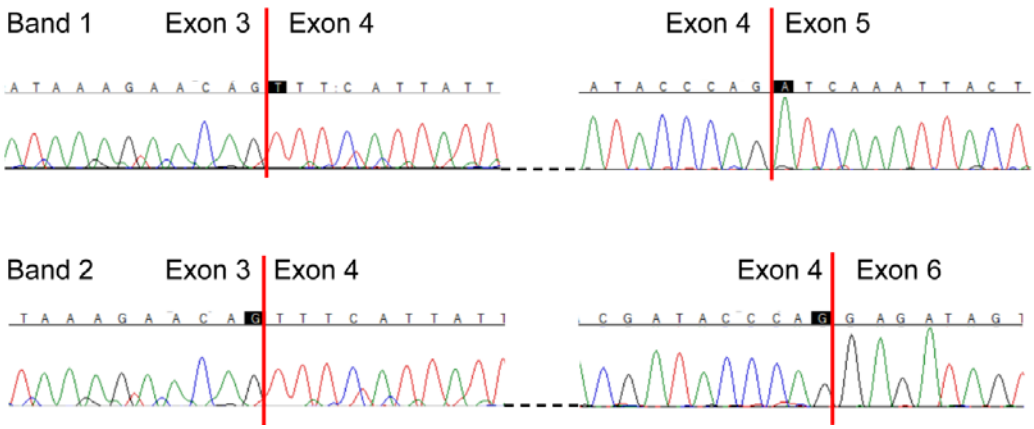

Figure S1. Family 12 segregates a genomic deletion encompassing exon 5 of *CDC45*.

(A) Manual interrogation of exome sequencing reads across the *CDC45* gene suggested a decrease in coverage across exon 5 in both affected samples and the carrier mother, compared to the father, who carries the c.893C>T, p.Ala298Val variant. While the reduction in coverage was not statistically significant, the presence of a rare variant on the *trans* allele in both affected samples prompted further investigation. BAM files visualized using IGV. (B) MLPA, comparing the quantity of DNA in a test sample vs a synthetic control with multiple probes across *CDC45*, was performed in both affected samples and the mother, and all samples showed a deletion of exon 5. (Bi) Peak traces of control (red) and affected (blue). (Bii) Calculated ratio of DNA. Both probes for exon 5 demonstrate an approximately 50% reduction, consistent with a heterozygous deletion of exon 5. Probes for exon 4 and exon 6 do not show a reduction, indicating the breakpoints for the deletion lie within intron 4 and intron 5, respectively. Reports generated using GeneMarker Software (SoftGenetics Inc.). (C) RT-PCR and sequencing of cDNA from carrier parents in Family 12. (Ci) RT-PCR of exons 3-6 in *CDC45* from cDNA derived from parents in Family 12. There is an increase in a lower migrating band in the mother, who carries the exon 5 deletion allele (a faint co-migrating lower band visible in all samples is caused by physiological skipping of exon 4, see figure 5). (Cii) Sequencing of each band from the maternal sample indicates the lower migrating band (labelled Band 2) comprises exons 3, 4 and 6, with complete skipping of exon 5, resulting in an in-frame transcript.

Table S1. Experimental details for next-generation sequencing undertaken in this study.

Family	Clinical Diagnosis/ Study Focus	Design	Library Kit	Platform	Analysis Software			Coverage	Filtering parameters	Control populations
					Mapping	Variant Calling	Annotation			
1	Craniosynostosis (SC_2930), clinical genome sequencing	Genome	NEBNext DNA Sample Prep Master Mix Set 1 Kit	Illumina HiSeq2000	BWA[1], Stampy (v1.0.12-1.0.22)[2]	Platypus (v.0.2.4)[3]	ANNOVAR[4]	28x	Minor allele absent	1000 Genomes, ESP
2	Craniosynostosis	Exome	TruSeq V2	Illumina HiSeq2000	Novoalign (Novocraft Technologies)	SAMtools (v0.1.19)	ANNOVAR	55x	Minor allele absent	1000 Genomes, ESP
4	Primordial dwarfism	Exome	SureSelect V4	Illumina HiSeq2500	BWA, Stampy	SAMtools, Dindel	Ensembl VEP	50x	MAF < 0.005, ≥ 1 deleterious consequence prediction	1000 Genomes, ESP
12	Diagnostic	Exome	SureSelect^{XT} V5	Illumina HiSeq2500	Custom in-house pipeline MAGPIE (based on BAM-MEM and GATK)			70x	SeattleSeq, LOVDplus	GoNL, 1000 Genomes

MAF, minor allele frequency; GoNL, genomes of The Netherlands.

Table S2. Primers and amplification conditions for resequencing.

Dideoxy-sequencing primers to confirm variants in the craniosynostosis cohort[a]				
Variant	Primers	Primer sequence 5′→3 ′ Forward	Reverse	Product size (bp)
c.226A>C c.318C>T	4F/4R	TAGTGATGAAGGAAAAGGGGCCTCCTCG	CTGTTCCCAGTCCCACAGGGTAGTCAG	314
c.469C>T	5F/5R	ACCACGTATGGTGTAACTCTGGTGCCTCAC	CTTGGCCTGGCAGGCTTCAGGATGAC	436
c.653+5G>A	8F/8R	CATGAGCCTTAGACTTCTCTGCTTCCTTAC	ATCACACACATACCCAGAAAGGGGCTGCA	240
c.677A>G	9F/9R	GAGAGAGGCCACCTGACTGAGGCAAG	CAGTCCTCACTTCTCAATAGGACCCTA	335
c.1487C>T	16F/16R	CATAGACAAAGAACCGGCGCTGCAAACTG	GACACTAGAGGCAAATACCACTCTACTCAG	223
Dideoxy-sequencing primers for *CDC45* in the MGS cohort[b]				
Exon(s)	Forward		Reverse	Product size (bp)
1-2	GATTTGGCGGGAGTCTTG		ACGCAGCACCCTCACCTC	382
3	TCTTTTCAAGGTAAATTGCTAATGTC		TGGAAATAGAATGCTGTGTCAAG	230
4	AGTGATGAAGGAAAAGGGGC		CCAAGAACACCAGGTGAGAC	274
5	TCAGCTTATTAGGAAATGATAAGATTC		CCACTGCCCTCAGTACACC	343
6	CTGGGCCTACTGACTTCTGC		TCACTTCAAGCTAGAATAACCTTTC	519
7	TTTTCCAAAATATTTGGCTTCC		AGGACACTGACCCCTGGAG	174
8	TCAAGTCCAGTCTGGCTGC		TTATGTGGCACTGACCAAGG	201
9	CCTCATTGAGCCCAGGTG		GTGGCTATGGTCAGGCTGTG	179
10	CTGCCTGGTAAGAGCTGGAG		ACCCACAGAGGGTGACAAAG	257
11-12	CCACCTGCTGGAGTTACGAG		CCCTTCACTTTAATGAACCTGG	610
13	GCAGTGAGAGCTTGCCCAC		CCCGTAACTGACCTCCCTG	293
14-15	CAAGCAAACTATTTGTGACTTTGG		GGAGCTCTCCAAGCACCTG	437
16-17	CTCTGAGTGTTGAGCTGGGG		AACTTGCTTGGTTCCAGGG	506
18	TTCTGTGCCCTGTCTTGTG		AGCAGGGCATCAGGGTC	199

	Primers for Fluidigm resequencing in the craniosynostosis cohort[c]		
ID	Forward	Reverse	Length (bp, excluding universal adaptors)
CDC45_1	ACACTGACGACATGGTTCTACAAGTCTTGACCGCCGCC	TACGGTAGCAGAGACTTGGTCTCCCCTCATCCCTTCCCCA	173
CDC45_2	ACACTGACGACATGGTTCTACACCTCGGACGTGGATGCT	TACGGTAGCAGAGACTTGGTCTCTCACTTGCTGTTCACCTCCT	186
CDC45_3	ACACTGACGACATGGTTCTACAGTCCAGAGCCAGGTGACG	TACGGTAGCAGAGACTTGGTCTCTGAAGGATCTTGCACGCAC	210
CDC45_4	ACACTGACGACATGGTTCTACAAGATAGGCTTTGAAAACACTCTCTCT	TACGGTAGCAGAGACTTGGTCTTGCTGTGTCAAGAAATTACAATTGAGTA	186
CDC45_5	ACACTGACGACATGGTTCTACAATGAAGACACTATATTCTTTGTGTGTGAC	TACGGTAGCAGAGACTTGGTCTTAGTCAGACACACACCTTACCAAG	167
CDC45_6	ACACTGACGACATGGTTCTACATCAGAGGCTTAGTGATGAAGGAAAA	TACGGTAGCAGAGACTTGGTCTATTGACGACATTGACTGGCCTAT	192
CDC45_7	ACACTGACGACATGGTTCTACACCGTAGAAAGAGGAGAGGCTTAATT	TACGGTAGCAGAGACTTGGTCTGATAGCTGTGAGAGACCCAAACT	215
CDC45_8	ACACTGACGACATGGTTCTACAGGCCTACTGACTTCTGCCAAA	TACGGTAGCAGAGACTTGGTCTGGCTTCTGGTGCTGGGAG	193
CDC45_9	ACACTGACGACATGGTTCTACAGTGCCACCCATACCTCTGAC	TACGGTAGCAGAGACTTGGTCTCCATGGTCTCTAATGGATGGCA	188
CDC45_10	ACACTGACGACATGGTTCTACACTTCCTGTACTGCTACTTCCTGTT	TACGGTAGCAGAGACTTGGTCTACATTTGAGGACACTGACCCC	164
CDC45_11	ACACTGACGACATGGTTCTACAGCCTTAGACTTCTCTGCTTCCTT	TACGGTAGCAGAGACTTGGTCTGTGGCACTGACCAAGGCA	145
CDC45_12	ACACTGACGACATGGTTCTACACATCATCTCACTCCATCCCCC	TACGGTAGCAGAGACTTGGTCTGCTATGGTCAGGCTGTGCA	200
CDC45_13	ACACTGACGACATGGTTCTACATTCCCGCCACAACCACC	TACGGTAGCAGAGACTTGGTCTCACCTGCTTTCCCTCCTGG	191
CDC45_14	ACACTGACGACATGGTTCTACACTGCCTGGTAAGAGCTGGAG	TACGGTAGCAGAGACTTGGTCTGAGTGTGTTCTCCTCATCCTCG	141
CDC45_15	ACACTGACGACATGGTTCTACATTCAAGCTGTGGTCTGTGCA	TACGGTAGCAGAGACTTGGTCTTTCTGGGATCTAGGGCAAGGA	194
CDC45_16	ACACTGACGACATGGTTCTACAGCTTGCATGCTCCTTGACTG	TACGGTAGCAGAGACTTGGTCTCTCCTGGAGCCGCTTCTG	144
CDC45_17	ACACTGACGACATGGTTCTACAGTCGGTGTGTGGTGACCTC	TACGGTAGCAGAGACTTGGTCTCTTTAATGAACCTGGATGTAATGAAGATAAATC	200
CDC45_18	ACACTGACGACATGGTTCTACAGCTGTGTTTGCTCCCATGAC	TACGGTAGCAGAGACTTGGTCTCAAACCCACAGCCCTCCT	207
CDC45_19	ACACTGACGACATGGTTCTACAAACTCGCCAAGAAGCAGCT	TACGGTAGCAGAGACTTGGTCTAGACGAAGCCACTGGTGC	161
CDC45_20	ACACTGACGACATGGTTCTACATTACCAAGAGTTCCTGACAAGCA	TACGGTAGCAGAGACTTGGTCTAATGGTCTGCTGGGTGGC	127
CDC45_21	ACACTGACGACATGGTTCTACACAGTGGCTTCGTCTGACCAT	TACGGTAGCAGAGACTTGGTCTGGCCAGCATCTAACTCCCC	201
CDC45_22	ACACTGACGACATGGTTCTACACTCTGAGTGTTGAGCTGGGG	TACGGTAGCAGAGACTTGGTCTGGACGAGTGGAAGCTGCTC	200
CDC45_23	ACACTGACGACATGGTTCTACACATGTCTTGTGTGTCAGCAGC	TACGGTAGCAGAGACTTGGTCTCCAGCCATGCCAACTTGC	187
CDC45_24	ACACTGACGACATGGTTCTACAGTGAGCAGCTTCCACTCGT	TACGGTAGCAGAGACTTGGTCTCTTCTCAAACGCCCTCCCAA	196
CDC45_25	ACACTGACGACATGGTTCTACATCCCTTCTCACGGCTGTTTTT	TACGGTAGCAGAGACTTGGTCTCCAAGTAGAAGCCTCCGTTGA	201

MLPA Primer Sequences[d]	
ID	Sequence
CDC45-EX4-5	GGGTTCCCTAAGGGTTGGAGGCCAGTCAATGTCGTCAATGTATA
CDC45-EX4-3	CAACGATACCCAGGTACTTTTTGTGTCTAGATTGGATCTTGCTGGCAC
CDC45-EX3-5	GGGTTCCCTAAGGGTTGGAGATAGGCTTTGAAAACACTCTCTCTCCAGGC
CDC45-EX3-3	CTTGTTCCAGTGTGACCACGTGCAATATACGTCTAGATTGGATCTTGCTGGCAC
CDC45-EX5B-5	GGGTTCCCTAAGGGTTGGAGCGCACACGGTTAGAAGAGGTGAGTTTGGGTCTCT
CDC45-EX5B-3	CACAGCTATCCCAGAGGAACTTGCACTCCCAGAGGTCTAGATTGGATCTTGCTGGCAC
CDC45-EX7-5	GGGTTCCCTAAGGGTTGGACTACGAGCAGTATGAATATCATGGGACATCGGTAAGTAT
CDC45-EX7-3	GAATAGGTGGAACTCACTATAAAGTTCTGACTCCAGGGGTCTAGATTGGATCTTGCTGGCAC
CDC45-EX5A-5	GGGTTCCCTAAGGGTTGGAGATGATGACCTTGAAGTTCCCGCCTATGAAGACATCTTCAG
CDC45-EX5A-3	GGATGAAGAGGAGGATGAAGAGCATTCAGGAAATGACAGTGTCTAGATTGGATCTTGCTGGCAC
CDC45-EX6-5	GGGTTCCCTAAGGGTTGGAGCTGTGGGGATAAATTCCTGGTGCATTTGCTCCACCTTTTGTT
CDC45-EX6-3	CTCTTTGTCCCTGTATCAGGAGATAGTGGAGCAAACCATGCGGTCTAGATTGGATCTTGCTGGCAC

[a]DNA was extracted from either venous blood collected into EDTA, lymphoblastoid cell lines or cultured fibroblasts established from skin biopsies obtained from the scalp incision at the time of surgical intervention. All DNA was extracted using the Nucleon Blood and Cell Culture (BACC) DNA extraction kit (Gen-Probe Inc.) according to the manufacturer's instructions. PCR amplification of DNA was performed in a volume of 20 µl, containing 15 mM TrisHCl (pH 8.0), 50 mM KCl, 2.5 mM $MgCl_2$, 100 µM each dNTP, 0.4 µM primers, and 0.75 units of FastStart Taq DNA Polymerase (Roche). Cycling conditions comprised a 5 min initial denaturation step at 94°C, followed by 35 cycles of 94°C for 30 s, annealing at 63˚C for 30 s and extension at 72°C for 30 s, with a final extension at 72°C for 7 min. For dideoxy-sequencing, amplified PCR products were treated with *ExoI* (NEB) and shrimp alkaline phosphatase (FastAP; Thermo Scientific) to remove PCR primers and dNTPs respectively, by incubating at 37˚C for 30 min, followed by 85˚C for 15 mins to denature the enzymes. Sequencing was then carried out using the BigDye Terminator v3.1 cycle sequencer system (Applied Biosystems).

[b]PCR amplification of DNA was performed in a volume of 10 µl, using ReddyMix PCR master mix with 1.5 mM $MgCl_2$ (Thermo Scientific), 0.5 µM primers and 10 ng DNA. Cycling conditions employed a touchdown approach and were as follows: 5 min initial denaturation step at 95°C , then 3 cycles of 94°C for 30 s, 65°C for 30 s, 72°C for 45 s, then 3 cycles of 94°C for 30 s, 62°C for 30 s, 72°C for 45 s, then 3 cycles of 94°C for 30 s, 59°C for 30 s, 72°C for 45 s with a final 35 cycles of 94°C for 30 s, 56°C for 30 s, 72°C for 45 s, then a final extension of 72°C for 10 min. Dideoxy-sequencing was performed as in [a].

[c]Primer pairs were designed to amplify 25 target regions of approximately 200 bp, covering all 19 exons and intron/exon boundaries for use with the Access Array™ IFC system (Fluidigm). Universal CS1 and CS2 adaptor sequences were included on the 5′ ends of all target-specific forward and reverse primers, respectively. Primers were multiplexed into pools of 4-5 optimised pairs, with a final concentration of 1 µM per primer. Amplicon tagging, thermal cycling using the Biomark HD™ system (Fluidigm) and product harvesting were performed following the manufacturer's instructions. Ion PGM™ sequence-specific adaptors and sample indexes were attached to each amplicon pool for DNA extracted from 48 individual craniosynostosis patients using a DNA Engine Dyad® Peltier thermal cycler (Bio-Rad). Indexed PCR products were pooled, purified with AMPure XP beads (Beckman Coulter Ltd.) and quantified using an Agilent High Sensitivity DNA Kit with the 2100 Bioanalyzer (Agilent Technologies, Inc) or

the 2200 TapeStation (Agilent Technologies) with a High Sensitivity D1000 ScreenTape. In total, 467 patient samples were processed for downstream sequencing applications. Pooled and indexed PCR products were sequenced using the Ion PGM™ System (Life Technologies Ltd.). Pooled libraries were diluted to a final concentration of 10 pM and emulsion PCR and enrichment were performed with the Ion PGM™ Template OT2 200 Kit (Life Technologies Ltd.) according to the manufacturer's instructions. Enriched target regions were sequenced with the Ion PGM™ Sequencing 200 Kit v2 for 125 cycles, using an Ion 318 chip.

Underperforming amplicons (CDC45_2, CDC45_3 and CDC45_24) were re-sequenced independently. PCR products were amplified from 40 ng DNA with Q5® Hot Start High Fidelity polymerase (NEB) in the recommended standard reaction mixture, with the inclusion of Q5 High GC Enhancer. Cycling conditions were denaturation at 98°C for 30 s, followed by 35 cycles of 98°C for 10 s, 60°C for 30 s and 72°C for 30 s, followed by a final extension at 72°C for 2 min. Amplification products were diluted 100-fold and used in a second PCR reaction to incorporate Ion PGM™ sequence-specific adaptors and sample indexes as above, for 9 cycles. Pooled samples were purified and sequenced for 100 cycles as described above, using an Ion 314 chip. Sequence read alignment and variant analysis were performed using the Ion Torrent platform-specific software v4.2.1. In total 361 samples fulfilled minimum coverage parameters (x10 reads) for all amplicons.

[d]The MLPA reactions were performed according to a protocol based on the methods described previously.[5, 6] Products were separated by capillary electrophoresis on the ABI 3130 (Applied Biosystems) and data analyzed using GeneMarker (SoftGenetics Inc). Threshold ratios for deletion and duplication were set at <0.75 and >1.3, respectively. The colored primer sequences are universal for the MLPA procedure.

Table S3. Primer sequences used for cDNA analysis of *CDC45*.

Target Primers	Primer sequence 5′→3′		Product size (bp)
	Forward	Reverse	
Exon 1-3	TCCGATTTCCGCAAAGAGTTCTACG	CAGCGTATATTGCACGTGGTCACA	138
Exon 3-4	GGTGGCAAGAACTTGAAACTG	ACATTGACGACATTGACTGGCCTAT	166
Exon 3-5	GGTGGCAAGAACTTGAAACTG	ATGTCTTCATAGGCGGGAAC	238/100 if exon 4 skipped
Exon 5-6	GTTCCCGCCTATGAAGACAT	CTCCTCCGCATGGTTTGCTC	137
Exon 2F-5R	GACGTGGATGCTCTGTGTGC	GCTTCTCAGAAGGCTCTGACC	394/301 if exon 3 skipped /256 if exon 4 skipped
Exon 2_3F-5_4R	AGATCCTTCAGGCCTTGTTCC	TAATTTGATCTGGGTATCGTTGTATAC	251
Exon 2_3F-5_3R	AGATCCTTCAGGCCTTGTTCC	TAATTTGATCTGTTCTTTATGCTCAAG	113
GAPDH	GGACTCCACGACGTACTCAGCGCCAGC	GTGGATATTGTTGCCATCAATGACC	213

Table S4. *In silico* prediction of mutation effects on canonical splice sites.

Patient(s)	Mutation	Allele	Sequence	MAXENT Score	Sum Difference	Sum Variation	Significance Threshold	Significant[a]
P3	c.653+5G>A	G (WT)	tcagtaagg	8.61	5.95	-69%	-30%	Yes – 5´ donor site lost
		A (MUT)	tcagtaaag	2.66				
P9-1 & P9-2	c.203A>G, p.Gln68Arg	A (WT)	caggtattg	8.35	3.48	-42%	-30%	Yes – 5´ donor site lost
		G (MUT)	cgggtattg	4.87				
P10	c.1440+14C>T	C (WT)	caggcgggt	0.81	-7.75	+1157%	+30%	Yes – cryptic 5´ donor site created
		T (MUT)	caggtgggt	8.56				

[a]Significance based on thresholds applied by prediction software, Alamut Batch (Interactive Biosciences Inc) and Human Splicing Finder.[7]

Table S5. *In silico* splicing predictions for synonymous mutations in *CDC45*.

Patient(s)	Mutation	Motif affected	Predicted Consequence
P1	c.318C>T, p. V106V	Multiple potential silencing motifs created	Skipping of exon 4
P9-1 & P9-2	c.333C>T, p.N111N	SRp40 exonic splice enhancer motif lost	Skipping of exon 4

Predictions calculated using Human Splicing Finder.[7]

References

1. Li, H., and Durbin, R. (2009). Fast and accurate short read alignment with Burrows-Wheeler transform. Bioinformatics *25*, 1754-1760.
2. Lunter, G., and Goodson, M. (2011). Stampy: a statistical algorithm for sensitive and fast mapping of Illumina sequence reads. Genome Res. *21*, 936-939.
3. Rimmer, A., Phan, H., Mathieson, I., Iqbal, Z., Twigg, S.R., Consortium, W.G.S., Wilkie, A.O., McVean, G., and Lunter, G. (2014). Integrating mapping-, assembly- and haplotype-based approaches for calling variants in clinical sequencing applications. Nat. Genet. *46*, 912-918.
4. Wang, K., Li, M., and Hakonarson, H. (2010). ANNOVAR: functional annotation of genetic variants from high-throughput sequencing data. Nucleic Acids Res. *38*, e164.
5. Schouten, J.P., McElgunn, C.J., Waaijer, R., Zwijnenburg, D., Diepvens, F., and Pals, G. (2002). Relative quantification of 40 nucleic acid sequences by multiplex ligation-dependent probe amplification. Nucleic. Acids. Res. *30*, e57.
6. White, S.J., Vink, G.R., Kriek, M., Wuyts, W., Schouten, J., Bakker, B., Breuning, M.H., and den Dunnen, J.T. (2004). Two-color multiplex ligation-dependent probe amplification: detecting genomic rearrangements in hereditary multiple exostoses. Hum. Mutat. *24*, 86-92.
7. Desmet, F.O., Hamroun, D., Lalande, M., Collod-Beroud, G., Claustres, M., and Beroud, C. (2009). Human Splicing Finder: an online bioinformatics tool to predict splicing signals. Nucleic Acids Res. *37*, e67.